Boise State University
ScholarWorks

CGISS Publications and Presentations

Center for Geophysical Investigation of the Shallow Subsurface (CGISS)

8-2-2004

Seismic Expression of Pleistocene Paleoceanographic Changes in the California Borderland from Digitally Acquired 3.5 Khz Subbottom Profiles and Ocean Drilling Program Leg 167 Drilling

Aleksandra Janik
University of Miami

Mitchell W. Lyle
Boise State University

Lee M. Liberty
Boise State University

Copyright 2004 by the American Geophysical Union. DOI: 10.1029/2003JB002439

Seismic expression of Pleistocene paleoceanographic changes in the California Borderland from digitally acquired 3.5 kHz subbottom profiles and Ocean Drilling Program Leg 167 drilling

Aleksandra Janik

Division of Marine Geology and Geophysics, Rosenstiel School of Marine and Atmospheric Science, University of Miami, Miami, Florida, USA

Mitchell W. Lyle and Lee M. Liberty

Center for Geophysical Investigation of Shallow Subsurface, Boise State University, Boise, Idaho, USA

Received 9 February 2003; revised 1 March 2004; accepted 28 April 2004; published 2 July 2004.

[1] We correlate processed 3.5 kHz seismic profiles with physical properties of cores collected during ODP Leg 167 from the Tanner, East Cortes, and San Nicolas Basins through much of the Pleistocene succession. Results indicate that seismic horizons in the unconsolidated Pleistocene sediments (top 50 m) are mainly controlled by density contrasts. Removing of the compaction trend from the density reveals a very interesting relationship between density and composition - the density closely and inversely correlates with organic carbon indicating that large-scale variations in organic carbon are responsible for seismic reflections through their influence on density. This is a significant discovery since there apparently is no other paleoceanographic setting that we know of where such a close linkage between acoustic properties and organic carbon has been established. The variations in organic carbon are mainly marine in origin and derive from variations in primary productivity associated with upwelling and the preservation regime related to oxygenation of water. Pleistocene reflections on 3.5 kHz profiles in the Borderland province thus record regional cyclical fluctuations in the paleoclimatic signals. The close resemblance in the density profiles at the three different basins indicates that the sedimentary regime was similar in those basins through the Pleistocene. These common density patterns produce regional seismic horizons that correlate well among the basins. It is likely these correlated and dated horizons could be extrapolated to other Borderland basins (e.g., San Clemente), where they can potentially be used as time markers for neotectonic studies in the region. *INDEX TERMS:* 0910 Exploration Geophysics: Data processing; 3022 Marine Geology and Geophysics: Marine sediments—processes and transport; 3025 Marine Geology and Geophysics: Marine seismics (0935); 4279 Oceanography: General: Upwelling and convergences; 5102 Physical Properties of Rocks: Acoustic properties; *KEYWORDS:* California Borderland, 3.5 kHz seismic data, ODP Leg 167, Tanner Basin, organic carbon

Citation: Janik, A., M. W. Lyle, and L. M. Liberty (2004), Seismic expression of Pleistocene paleoceanographic changes in the California Borderland from digitally acquired 3.5 kHz subbottom profiles and Ocean Drilling Program Leg 167 drilling, *J. Geophys. Res.*, *109*, B07101, doi:10.1029/2003JB002439.

1. Introduction

[2] A seismic reflection image of a sedimentary basin derives from a complex interplay between geology (paleoenvironmental factors, tectonic events, diagenesis/lithification) and the input seismic pulse. Ideally, the seismic record can be used to determine the spatial extent of lithologic units and ascertain if lithologic changes in a borehole are regionally significant. The primary objective of this study was to identify the relationship between paleoceanographic changes, sedimentation and the seismic reflection record in the California Borderland region over the last 500 k.y. This discussion focuses on the high-resolution seismic record obtained from digitally-recorded 3.5 kHz signals because the data obtained with 80 in^3 (1311cm^3) waterguns lack the resolution and detail to address this objective. We develop the link between the 3.5 kHz seismic reflections and changes in sediment composition, and then tie this seismic record to a timescale based on oxygen isotope stratigraphy. We conclude with a discussion of the paleoceanographic significance of the seismic horizons.

[3] Previous work in the California margin area includes studies of the Neogene marine sedimentary record using conventional seismic reflection profiles collected by academia and drilling and seismic data collected by industry

Copyright 2004 by the American Geophysical Union.
0148-0227/04/2003JB002439$09.00

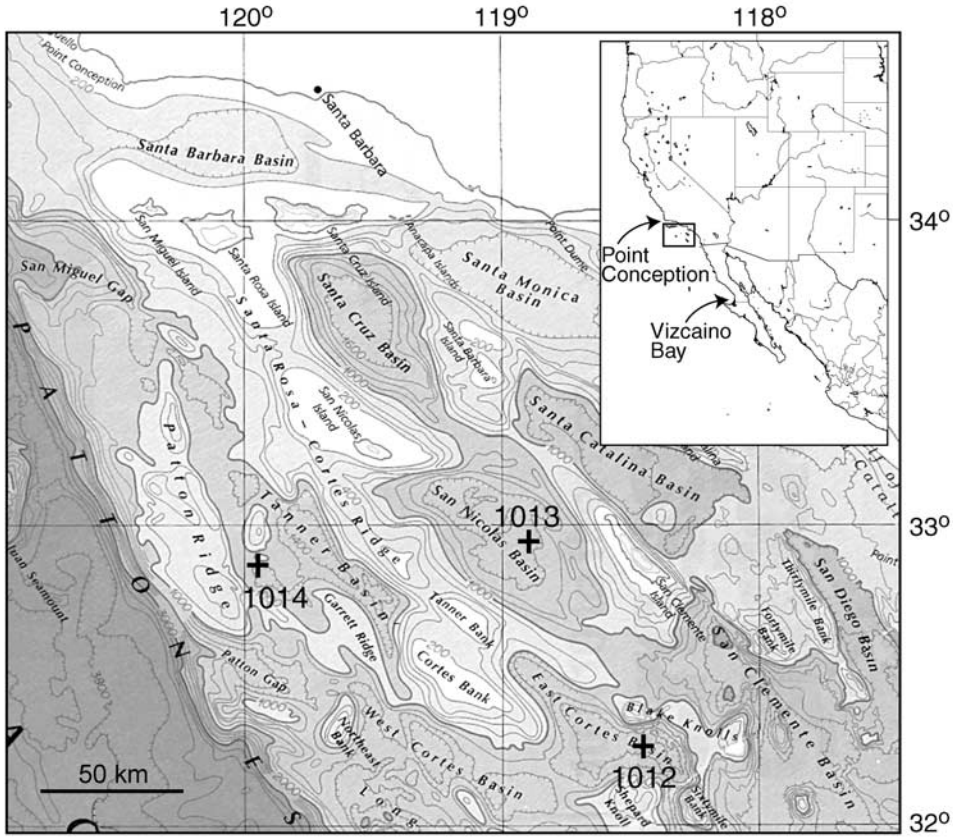

Figure 1. Map of the northern California Borderland basins with locations of Ocean Drilling Program (ODP) Site 1012, East Cortes Basin; ODP Site 1013, San Nicolas Basin; and ODP Site 1014, Tanner Basin. Inset: General map of the California Borderland, which extends from Point Conception to Vizcaino Bay.

[*Teng and Gorsline*, 1991; *Vedder*, 1987; *Victor*, 1997; *Dunkel*, 2001] (see http://www.scec.org/borderland/). Additional insight into the Neogene sedimentary sequence has come from seismic profiles collected primarily by the USGS to investigate California earthquake hazards [*Normark et al.*, 1999; *Gumacher et al.*, 2000]. There is also good knowledge of late Pleistocene and Holocene sedimentary processes revealed in piston and gravity cores [*Emery*, 1960; *Gorsline et al.*, 1968; *Schwalbach and Gorsline*, 1985; *Mortyn et al.*, 1996]. However, because of high sedimentation rates in this region these cores were too short to define the complete history of Pleistocene sedimentation. This is now possible using results of Ocean Drilling Program Leg 167 [*Lyle et al.*, 1997].

2. Tectonic and Oceanographic Setting

2.1. Overview of the Study Area

[4] The California Borderland basins (Figure 1, inset) extend along a 1000 km section of the East Pacific margin between Point Conception and Vizcaino Bay [*Gorsline and Teng*, 1989]. The seaward edge of the California Borderland is the Patton Escarpment. With over twenty basins, the Borderland province encompasses about 120,000 km^2 [*Emery*, 1960]. In this study, we focus on three outer basins (Figure 1) (East Cortes Basin (Site 1012), San Nicolas Basin (Site 1013) and Tanner Basin (Site 1014)) cored during ODP Leg 167 [*Lyle et al.*, 2000]; distances of the basins from shore are about 105, 115, and 155 km, respectively, and their water and sill depths are 1783/1415, 1575/1106, and 1177/1165 m.

2.2. Tectonic Setting

[5] The California Borderland province consists of a series of semi-enclosed basins and banks or islands located offshore southern California [*Emery*, 1960]. It is part of the complex plate boundary between the Pacific and North American plates, which variously experienced subduction, rifting and transform faulting within a relatively short period of time (Oligocene to the present) [e.g., *Legg et al.*, 1991; *Legg*, 1991; *Crouch and Suppe*, 1993; *Bohannon and Parsons*, 1995; *Bohannon and Geist*, 1998; *Zhang et al.*, 1998; *ten Brink et al.*, 2000; *Miller*, 2002]. The crustal structure of the inner California Borderland basins has been investigated through gravity modeling and deep seismic reflection and refraction experiments such as the Los Angeles Region Seismic Experiment (LARSE) [*Brocher et al.*, 1995]. The origin of the inner Borderland region has been interpreted as a metamorphic core complex underlain by a crustal-scale thickness of Catalina Schist. A continuing debate concerns whether a lower crustal layer of subducted oceanic crust is present [*ten Brink et al.*, 2000]. Little is known about the outer Borderland deep crustal structure.

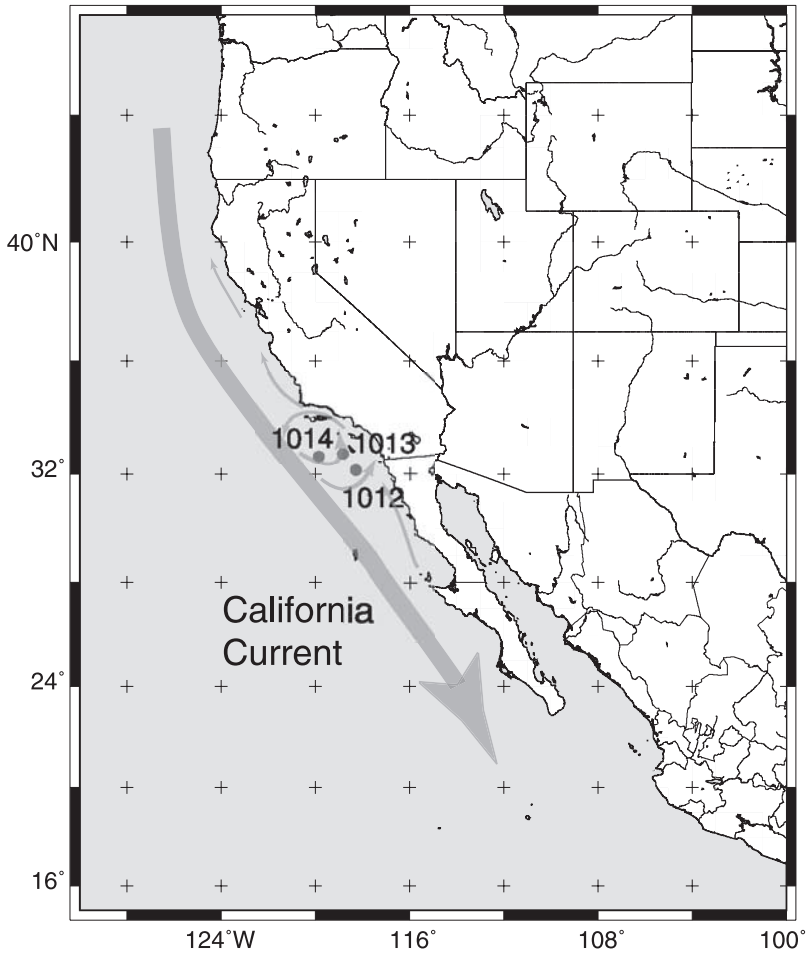

Figure 2. Schematic flow of the California Current and its eddies.

[6] The dominant structural trend of the Borderland basins is NW-SE, parallel to the current relative motion between plates. Basinal morphology is the result of interaction between the East Pacific Rise and the North American Plate, and the primary driving force for the current deformation is the relatively rapid NW motion of the Pacific Plate. Beginning in the Oligocene, the East Pacific Rise was overridden by the North American plate and subduction activity was replaced by transform fault tectonism [*Atwater*, 1989]. Eventually, a piece of continental margin was transferred to the Pacific Plate, forming the California Borderland [*Teng and Gorsline*, 1991]. Basin geometries originally were influenced by Miocene and Pliocene extension and rotation of the Borderland [*Bohannon and Geist*, 1998]. Most of the Miocene activity involved normal faulting, with some exceptions in the Santa Cruz and San Nicolas Basins, where late-stage Miocene transpression formed some reverse faults [*Victor*, 1997]. Subsequent transform activity starting in the late Miocene migrated inland and is presently accommodated by the San Andreas, Elsinore and San Jacinto faults in Southern California. At least several mm/yr of strike-slip displacement is still accommodated in the Borderland today and modern tectonic activity is being probed by various GPS and satellite remote-sensing studies [*Feigl et al.*, 1993; *Ward and Valensise*, 1996; *Dixon et al.*, 2000; *Prawirodirdjo and Bock*, 2001]. Strike-slip motion is accompanied by some compression in Borderland (as in the rest of California) leading to inversion of some of the previously extensional features.

2.3. Oceanographic Setting

[7] The California Borderland basins lie below the highly productive waters associated with a major eddy in the California Current (Figure 2). The California Current, with its cool and relatively fresh waters, is the eastern boundary current of the north Pacific surface gyre, which flows southward past California to the equatorial area [*Lynn and Simpson*, 1987]. The strength of the California Current varies both seasonally and interannually. The seasonal variations are controlled by changes in the coastal winds, whereas the interannual variations are caused by fluctuations of the north Pacific surface gyre and by teleconnection to the tropics via ENSO (El Niño-Southern Oscillation) and PDO (Pacific Decadal Oscillation) [*Pares-Sierra and O'Brien*, 1989]. Consequently, California Current structure reflects both local wind variations and basinwide surface pressure conditions within the north and equatorial Pacific.

[8] The California margin coastal upwelling system is forced by atmospheric circulation around the North Pacific high-pressure regime, which varies seasonally both in strength and position. Ekman transport is less intense in the Borderland than along the adjacent regions to the south

and north due to the offshore position of the California Current and the unfavorable orientation of the coastline relative to the winds [*Huyer*, 1983]. However, because of the complex interaction between the curl of wind stress, the California Current, and irregularities in the Borderland bathymetry, there is a strong seasonal upwelling in the Borderland as well.

[9] On much longer timescales, the sea surface temperature (SST) regime along the California margin varies in response to ice age cycles. The total amplitude of the SST change in the California Borderland region from glacial to interglacial cycles has been estimated based on alkenone unsaturation indices to be about 8–9° [*Herbert et al.*, 2001]. The coldest temperatures generally preceded glacial maxima by 5–10 k.y. in each glacial cycle, which has been interpreted as a weakening of the California Current at glacial maxima.

2.4. Sedimentation

[10] Sedimentary input to the Borderland basins can be viewed as a multicomponent and multivariant process dependent upon paleoceanographic and tectonic factors. The inner basins of the California Borderland are filled for the most part with turbidites, but the outer basins and tectonic highs are dominated by hemipelagic sedimentation. The main paleoceanographic influence on the sedimentation in the outer borderland, where Sites 1012, 1013, and 1014 are located, is upwelling. This produces a relatively continuous pelagic biogenic rain of calcareous and siliceous material in various proportions. Instabilities in the ''rain'' derive from changes in the physical oceanography, such as variations in wind stress that affect the upwelling intensity [*Ravelo et al.*, 1997]. Another important source of the Quaternary succession is terrigenous clay. The organic matter flux to the outer basins is mainly of marine provenance, with episodic input of terrigenous organic matter in the basins with closer proximity to land. Some of the marine organic carbon is deposited in laminated sediments found in several contemporary depositional environments throughout the Borderland, probably representing the millennial-scale oscillation of bottom-water oxygen content [*Bull and Kemp*, 1996; *Gorsline et al.*, 1996; *Behl and Kennett*, 1996; *Pike*, 2000].

[11] The terrigenous component derives from rivers or via wind and surface ocean current transport. Significant quantities of clay are brought from the north by the California Current. Riverine discharge introduces both clastics and terrigenous organic material that disperses widely from a limited number of point sources (e.g., the Santa Clara River) [*Gorsline and Teng*, 1989; *Marsaglia et al.*, 1995]. An important aeolian component is fine dust blown from interior desert basins by the Santa Ana winds. Aeolian transport also introduces some volcanic glass into the basins. The volcanic glass occurs disseminated throughout the section or as distinct ash layers [*Lyle et al.*, 1997].

[12] Finally, tectonic events arising directly or indirectly from seismicity introduce periodic mass transport deposits such as turbidites and slumps, especially in the inner California Borderland basins [*Lyle et al.*, 1997]. The turbidites are composed mainly of quartz and feldspar sand and foraminifers shells, and are likely to have originated on the nearby bathymetric highs. Exotic fragments such as carbonaceous wood fragments are occasionally found in the turbidites.

[13] The resulting Quaternary sedimentary sequence at the investigated sites in the East Cortes (Site 1012), San Nicolas (Site 1013), and Tanner (Site 1014) Basins of the outer California Borderland is composed of variable amounts of silty clay, nannofossils, foraminifers, organic carbon and volcanic glass, with trace quantities of sponge spicules, diatoms, radiolarians, opaque minerals and pyrite [*Lyle et al.*, 1997].

3. Data Collection and Processing

[14] For this study we mainly rely on digitally-recorded 3.5 kHz subbottom reflection profiles. The watergun seismic data are used only to provide generalized images of the depositional style of the region because of their lack of adequate vertical resolution. The core datasets consist of physical and geochemical properties measured on recovered material. These include sediment density, porosity, and composition. Oxygen isotope data measured from foraminifera separated from cored sediments are used to establish the geological chronology and to correlate geochemical data to the global ice-volume signal.

3.1. Sediment Physical and Chemical Properties

[15] GRAPE (Gamma Ray Attenuation Porosity Estimator) bulk density data for the cores [*Boyce*, 1976] were measured using a shipboard Multi Sensor Track (MST) with an average measurement spacing of 4 cm. This spacing represents about 500 years of deposition, assuming an average sedimentation rate of 80 m/m.y., which is typical of the outer Borderland basins [*Ravelo et al.*, 1997]. The GRAPE sensor provides an almost continuous log of approximate wet bulk density. Actual density measurements of discrete samples, though collected with much lower resolution, were also used in this study to compare with geochemical composition and porosity data collected on the same samples.

[16] P wave velocity measurements were attempted using the MST, but the high gas content of the sediments created expansion cracks and unacceptable levels of attenuation of the elastic pulse [*Slowey and Bryant*, 1995; *Tuffin et al.*, 2000], thus preventing direct velocity determinations from the cores, so the lack of velocity measurements is entirely due to the measurement problems. Downhole logging at Site 1014 was only obtained below a depth of 58 mbsf, thus excluding the 0–500 ka study interval. This is because typically 50–100 m of drill string is left in the hole to stabilize it.

[17] The shipboard low resolution carbonate concentrations were calculated from the inorganic carbon content determined using a Coulometrics 5011 carbon-dioxide coulometer [*Lyle et al.*, 1997] with the assumption that all inorgranic carbon is present as calcium carbonate. The shipboard total organic carbon (C-org) data were obtained by subtracting the inorganic carbon from the total carbon values, which were acquired by gas chromatography of the combusted sediments using a Carlo Erba 1500 CN Analyzer. These low resolution $CaCO_3$ and C-org data were collected about every 1.5 m on the same samples from which discrete bulk density and porosity data were gathered.

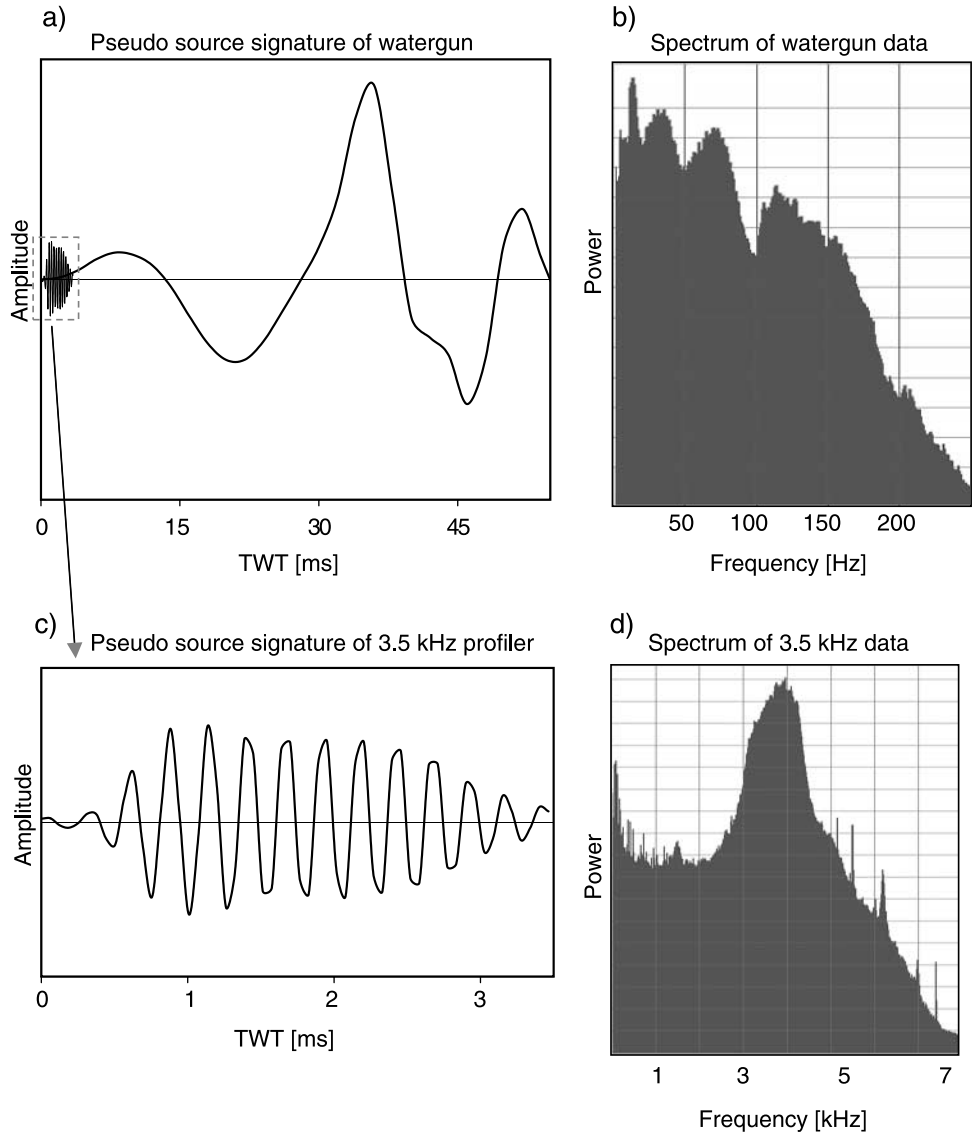

Figure 3. Parameters of seismic data acquisition. (a) Pseudo source signature (from the direct wave arrival) of the 80 in^3 (1311 cm^3) watergun (bold line) and 3.5 kHz source (thin line). Amplitude of watergun signal is much stronger that that of 3.5 kHz profiler, although the relationship is not to scale here. Watergun source signature was obtained by averaging 10 direct wave arrivals to one channel. (b) Spectrum of the watergun data for one channel. (c) Pseudo source signature of the 3.5 kHz profiler obtained from clean seafloor reflections. (d) Spectrum of the 3.5 kHz data.

[18] The geochemical dataset was expanded during post-cruise work at Boise State University, where high resolution measurements of C-org (using acidification with 10% HCl) and $CaCO_3$ (by difference between the total carbon and C-org, multiplied later by 8.33) were collected from Site 1012 (East Cortes) at a 4 cm sample spacing [*Lyle et al.*, 2000]. Oxygen isotope data were also acquired during post-cruise research [*Hendy and Kennett*, 2000; *Andreasen et al.*, 2000] (A. C. Ravelo, personal communication, 2000).

[19] Shipboard sedimentological analysis [*Lyle et al.*, 1997] indicates that, beside carbonates, silty clay is another major sedimentary component, so clay content was estimated by subtracting the calcium carbonate and organic carbon weight percent from 100%.

[20] Siliceous microfossils are not present in any significant amount at Sites 1012 and 1013 [*Lyle et al.*, 1997; *Janecek*, 2000] and at Site 1014 the small quantities of opal did not have a substantial influence on density. Opal is thus not included in this discussion.

3.2. Data Processing and Image Enhancement of 3.5 kHz Subbottom Profiles

[21] The 3.5 kHz subbottom profiles were digitally recorded on board the R/V *Ewing* during the EW9709 cruise. A Geometrics R-series seismograph was used to record the data at a 0.064 ms sample rate. Pre-processing involved attenuating the analog signal (±12V) to match the ±5 volt limit of the digital recording system. The resulting signal bandwidth of the data extended from

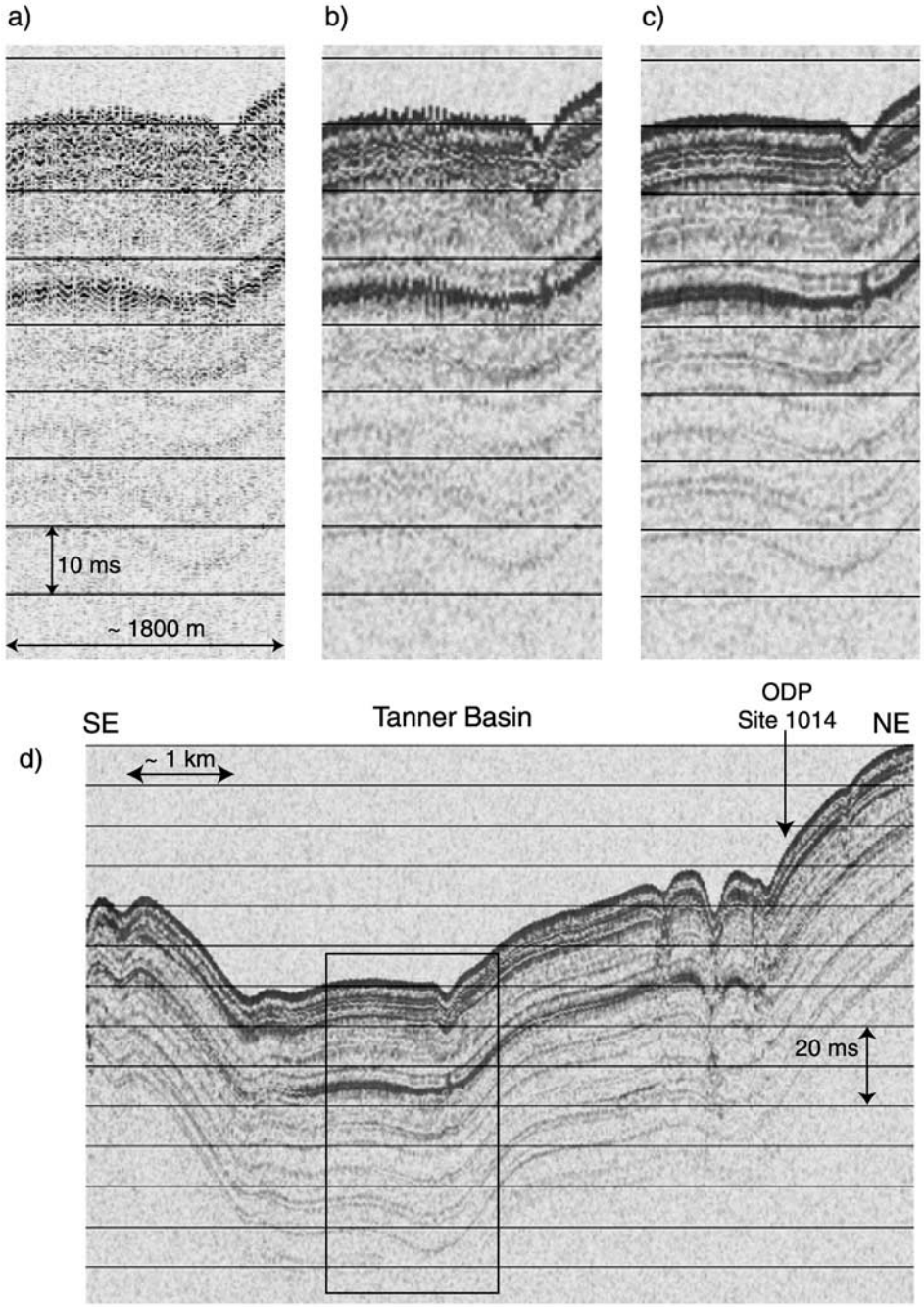

Figure 4. Processing steps for the 3.5 kHz subbottom profiles. (a) Raw data. (b) Reflection strength display (instantaneous amplitude). (c) Reflection strength display and seafloor smoothing procedure. (d) Complete processed 3.5 kHz profile from the Tanner Basin. Rectangle shows the position of the section used for the detailed display of the processing steps.

about 3.0 to 4.5 kHz (Figure 3d), and the signal penetrated to about 50 meters below seafloor (mbsf) with submeter resolution.

[22] Unlike analog 3.5 kHz profiles, the digitally acquired information allows us to process it in ways that improve the clarity of the seismic image and reflection definition (Figure 4), consequently optimizing the ability to successfully correlate to the drill-hole information.

[23] A sample of the unprocessed 3.5 kHz data is shown in Figure 4a. The image is not clear and most seismic horizons are vague. Data was processed to produce reflection strength displays, also called amplitude envelopes or instantaneous amplitudes [*Taner et al.*, 1979]. Although the lateral continuity of reflectors was immediately improved (Figure 4b), some of the vertical resolution was lost because the absolute value of the complex trace amplitude was used (Figure 5). The term ''instantaneous'' indicates that the attribute is calculated for every value of the trace, which tends to emphasize the very fine changes in data character from sample to sample. These attributes have found multi-

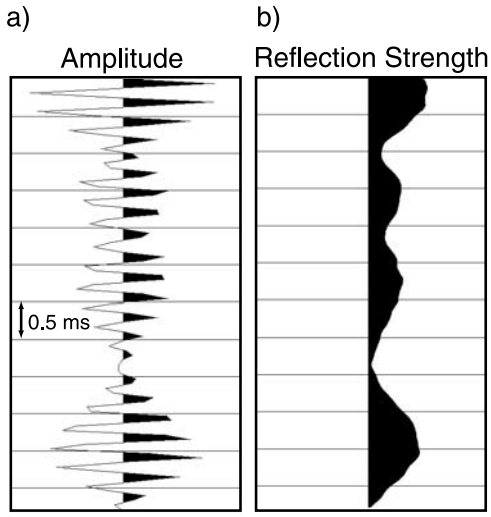

Figure 5. Influence of the reflection strength display on vertical resolution of 3.5 kHz profile. (a) Seismic trace in a conventional amplitude display. (b) Reflection strength display; reflections are enhanced but resolution is slightly compromised. The TWT interval of 0.5 ms equals to 0.375 m assuming the velocity of 1500 m/s.

ple applications in geophysics [*Bodine*, 1984; *Brown*, 1999] because the subtle wavelet distortions they emphasize are often caused by stratigraphic changes such as pinch-outs, thin beds, lateral change of facies, and gas/oil/water boundaries [*Chen and Sidney*, 1997]. In this study, we found the reflection strength display useful because it enhanced the amplitude features and thus improved the definition of horizons.

[24] Programs to calculate instantaneous attributes are included in the more common seismic data processing and interpretation software packages, so reflection strength can be quickly and easily displayed. For this work the instantaneous amplitude image was computed and plotted using the ProMAX seismic processing system.

[25] The remaining trace-to-trace jitter (zigzag pattern) in Figure 4b is mainly caused by ship heave (wave motion). Because of the high resolution nature of the data set, although the seas were calm, ship motion caused significant differences in the first arrival time from trace to trace on the order of one dominant wavelength. This noise was removed by applying a 5-point boxcar filter to the first arrival horizon and adjusting each trace to this level via the flattening and the unflattening processing procedures in ProMAX. This simple technique greatly improves the coherency of the seafloor reflection and the later arrivals, without affecting the amplitude content (Figures 4c–4d).

3.3. Conventional Seismic Reflection Data Processing

[26] Four-channel seismic reflection data were collected in the California Borderland region in 1995 using twin 80 in^3 waterguns during the site survey cruise EW9504 on R/V *Ewing* [*Lyle et al.*, 1995]. The average shot spacing was about 36 m, the sample rate was 2 ms, and a 160 Hz high-cut analog field filter was applied to all of the data (Figures 3a–3b). The resulting seismic data underwent the standard processing sequence that included spherical divergence correction, stacking, bandpass filtering, and spiking deconvolution.

4. Adequacy and Limitations of the Seismic Data as Tools for Pleistocene Paleoceanographic Studies

[27] Although the energy of the watergun seismic source is about 10^5 J, the dominant frequency of the watergun data is only about 50 Hz. In comparison, the energy of the 3.5 kHz source is only about 10–20 J, but the dominant frequency about 3600 Hz. Because of the trade-off between seismic penetration depth and seismic frequency [*Sheriff and Geldart*, 1995; *Mosher and Simpkin*, 1999], these parameters translate into the following: The watergun data penetrate hundreds to thousands of meters, but are limited to a best-case reflector resolution of about 9 m in the section of interest here. The 3.5 kHz data only penetrate the upper 50 m of the section, but offer a best-case resolution of about 11 cm. Figure 6 clearly portrays the penetration difference. The Pleistocene section in the California Borderland is typically represented by about 100 m of sediment cover, so the 3.5 kHz data generally penetrate a significant portion of the Pleistocene.

[28] The vertical resolutions computed above utilize the quarter-wavelength assumption [*Yilmaz*, 2001; *Widess*, 1973] and assume a P wave velocity of about 1500 m/s (representative for unconsolidated marine sediments) (Tables 1 and 2). In practice, the resolutions may be worse than computed above, especially in difficult field conditions during data collection.

[29] The ability to resolve the appropriate geological time intervals depends not only on the innate resolving power of the seismic method but also on the sediment P wave velocity and sedimentation rates. Tables 3 and 4 theoretically quantify this problem for various combinations of seismic frequencies, sedimentation rates, and durations of geological episodes.

[30] In practice there are additional factors that decrease the vertical resolution. These result from noise in the seismic data, the complexity of the source signature shape, and seismic processing (e.g., using the reflection strength display that enhances reflection clarity but introduces some loss of detail and reduces resolution by factor 2–3; Figure 5). Consequently, the actual resolution is lower than the theoretical quarter of one wavelength. For integration of the 3.5 kHz profiles with core data, a further decrease in quality is introduced by the measurement error of acoustic core properties. An appropriate example of this can be found in collection of GRAPE density data, which is a very fast process that yields high resolution data, but also data that tend to be noisy due to sensitivity of GRAPE sensor to any cracks, voids and imperfect contact between the sediments and the plastic liner. This instrumental noise is eventually inherited by the impedance and reflection coefficient profiles during computing of the convolution. All of the abovementioned factors intertwine to decrease the quality of the integration of high resolution seismic and borehole data.

[31] Nevertheless, the 3.5 kHz profiler certainly offers submeter vertical resolution, which should be adequate to

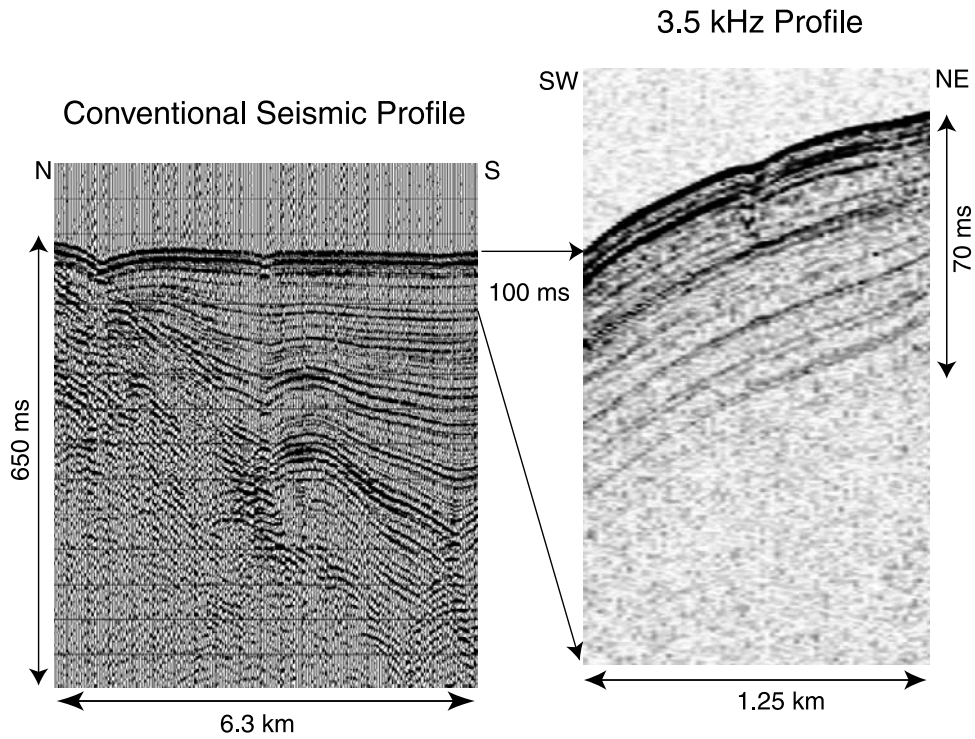

Figure 6. Comparison of penetration depth of conventional 4-channel seismic data and 3.5 kHz high resolution profile. The TWT interval of 70 ms equals to 52.5 m assuming the velocity of 1500 m/s.

study Pleistocene sedimentation in APC (Advanced Piston Core) sections of drillsites in the California Borderland.

5. Integration of Borehole Data with 3.5 kHz Profiles

5.1. General

[32] Simplistically, a seismic reflection is produced when a change in lithology produces a sufficiently abrupt contrast in acoustic impedance to reflect acoustic energy back to the receiver [*Robinson et al.*, 1986; *Sheriff and Geldart*, 1995]. The acoustic impedance is a product of the sediment bulk density (ρ) and P wave velocity (v). The amount of seismic energy reflected by the interface between layer n and n + 1 is determined by a reflection coefficient (R) representing the acoustic impedance contrast (1):

$$R = \left(\rho_{n+1} v_{n+1} - \rho_n v_n\right) / \left(\rho_{n+1} v_{n+1} + \rho_n v_n\right). \quad (1)$$

[33] As an acoustic wave front propagates into the subsurface, the amplitude of the wave decreases because of geometric spherical divergence, scattering, attenuation, and the partitioning of transmitted and reflected energy. The frequency content of the signal is also affected with higher frequencies attenuated more quickly than lower frequencies by sediment/pore fluid interactions [*Biot*, 1956a, 1956b; *Murphy et al.*, 1986; *Peacock et al.*, 1994; *Leurer*, 1997; *Sams et al.*, 1997]. Consequently, both amplitude and frequency change during transmission of the seismic signal.

Table 1. Vertical Resolution for Seismic Source of Dominant Frequency F = 50 Hz

Seismic Velocity V, m/s	Wavelength λ = V/f, m	Vertical Resolution R = λ/4, m
1460	29.20	9.13
1480	29.60	9.25
1500	30.00	9.38
1550	31.00	9.69
1600	32.00	10.00

[34] The geological nature of what causes impedance contrasts is very complicated. Virtually any intrinsic rock property can play a role, as long as it results in a change in density or P wave velocity. These range from sediment composition to packing, grain density-velocity to composite density-velocity, porosity, diagenesis, lithification, age, abundance and type of microfossils present. However, in unconsolidated marine sediments, changes in the sediment wet bulk density rather than velocity is the principal variable controlling the acoustic impedance profile [*Mayer et al.*, 1985; *Slowey et al.*, 1996]. Before sediment become more consolidated, P wave velocity remains within roughly ±3% of an average value. In contrast, wet bulk density can vary by as much as ±30% with major changes in lithology and porosity.

5.2. Correlation of Density and 3.5 kHz Profiles at Sites 1013 and 1014

[35] We can link the 3.5 kHz profiles and borehole data by comparing the reflection coefficient profile derived from the core to the 3.5 kHz profiles of instantaneous amplitude at Sites 1013 and 1014. Site 1012 does not have

Table 2. Vertical Resolution for Seismic Source of Dominant Frequency F = 3.5 kHz

Seismic Velocity V, m/s	Wavelength λ = V/f, m	Vertical Resolution R = λ/4, m
1460	0.42	0.104
1480	0.42	0.106
1500	0.43	0.107
1550	0.44	0.111
1600	0.46	0.114

Table 4. Geological Time Corresponding to 10.6 cm Vertical Resolution (3.5 kHz Source)

Sedimentation Rate, m/m.y.	Geological Time, k.y.
30	3.53
60	1.77
80	1.33
100	1.06

digital 3.5 kHz images available. Although synthetic seismograms are often used for this task, we did not to use this method directly because of high noise level in the synthetic seismogram. This was caused by convolution of the pseudo source signature derived from the data (seafloor reflection, Figure 3c), which is only a rough estimate of the real source signal, with a reflection coefficient based on GRAPE density, which is characterized by the presence of high frequency measurement noise. Convolution of these two signals produces very noisy outputs because the frequency of the noise is close to the frequency of the signal. Additionally, the 3.5 kHz data at Site 1013 (Figure 7) were more noisy than at Site 1014 (acquisition problems), so the synthetic was prepared for Site 1014 only and the reflectors were approximately correlated. The final correlation between seismic and core data was done through the reflection coefficient profile (Figure 8).

[36] The reflection coefficient profiles were calculated based on smoothed GRAPE density (24 cm smoothing interval) for Sites 1014 and 1013 and then converted from depth to two way travel time (TWT) using the best estimate of constant velocity that provides the closest match between horizons and the reflection coefficient peaks and is still consistent with previously reported velocity values in similar sediments. The seismic velocity was chosen based on previous velocity studies in marine sediments [e.g., *Hamilton and Bachman*, 1982], which concluded that velocities for unconsolidated marine clayey sediments in same porosity range as the upper 50 m at Sites 1013 and 1014, are similar to the velocity of seawater. Additionally, some discrete velocity data are available from the southern part of the outer California Borderland collected on sediments drilled in the Animal Basin (Site 1011), and the velocity there varies from 1500–1540 m/s over the depth range of 0 to 40 m [*Lyle et al.*, 1997]. These data can be considered reliable because they did not suffer the methane gas expansion problems encountered at Sites 1012, 1013, and 1014. A final factor taken into account for the velocity estimate was velocity dispersion – the physical phenomenon describing velocity dependence on the frequency of the propagating wavelet. Because a higher frequency wave will have a higher propagation velocity, the velocity measurements performed on small discrete samples using 500 kHz frequency transducers most likely yield higher velocity values than the 3.5 kHz seismic velocities. Considering all aforementioned factors, a velocity of 1480 m/s was chosen for our approximate depth-to-time conversions at Site 1014 and 1500 m/s for Site 1013.

[37] We next compared the reflection coefficient profiles to the 3.5 kHz images and correlated several horizons. The peaks of the reflections were matched to maximum values of the reflection coefficient. Caution is required because indisputable correlation of reflection coefficient peaks to seismic horizons on a 3.5 kHz profile would be possible only with precisely known values of propagation velocity.

[38] At Site 1013 the quality of 3.5 kHz data is low and only the strongest reflectors were visible through the noise (Figure 7). At Site 1014 more reflectors could clearly be matched between the drill core and the 3.5 kHz profile (Figure 8, Table 5). These correlations demonstrate that the major acoustic impedance variations occur in the sediment cores from Sites 1013 and 1014 at a frequency resolvable by 3.5 kHz data, and confirm that the density variations (Figures 9a and 9b) cause seismic reflections in the 2.0–5.0 kHz frequency range in the upper 50 mbsf.

5.3. Comparisons Among Sites in the Search for Regional Reflectors

[39] We have established the link between high resolution seismic profiles and borehole data in San Nicolas Basin (Site 1013) and Tanner Basin (Site 1014) Basin by showing that major reflection coefficient peaks correlate with reflectors. The reflection coefficient peaks reflect steep density gradients, which are actual sediment properties. Unfortunately, there are no 3.5 kHz data at Site 1012, so bulk density data were compared between the 3 sites to identify potentially regional reflectors. Prior to doing so, the three density profiles (Figure 9b) had to be placed in the same normalized depth scale to make sure that the we compare features that occurred at the same geological time. This scale was developed by correlation between stable oxygen isotope data available at Sites 1012 and 1014 (Figure 10) using the AnalySeries software (D. Paillard et al., Macintosh Program Performs Time-Series Analysis, available at http://www.agu.org/eos_elec/, 1996). At Site 1013 oxygen isotope data were not available, but a minor linear stretch of the depth scale (37 mbsf at Site 1013 corresponds to 42 mbsf at Site 1014) made the Site 1013 density profile match the density at Site 1014. In addition, the density curves (sampled at every 4 cm) were subjected to a low-pass spatial frequency filter approximately equivalent to 6 point smoothing. This was done to enhance the major features

Table 3. Geological Time Corresponding to 9.25 m Vertical Resolution (50 Hz Source)

Sedimentation Rate, m/m.y.	Geological Time, k.y.
30	308
60	154
80	116
100	92

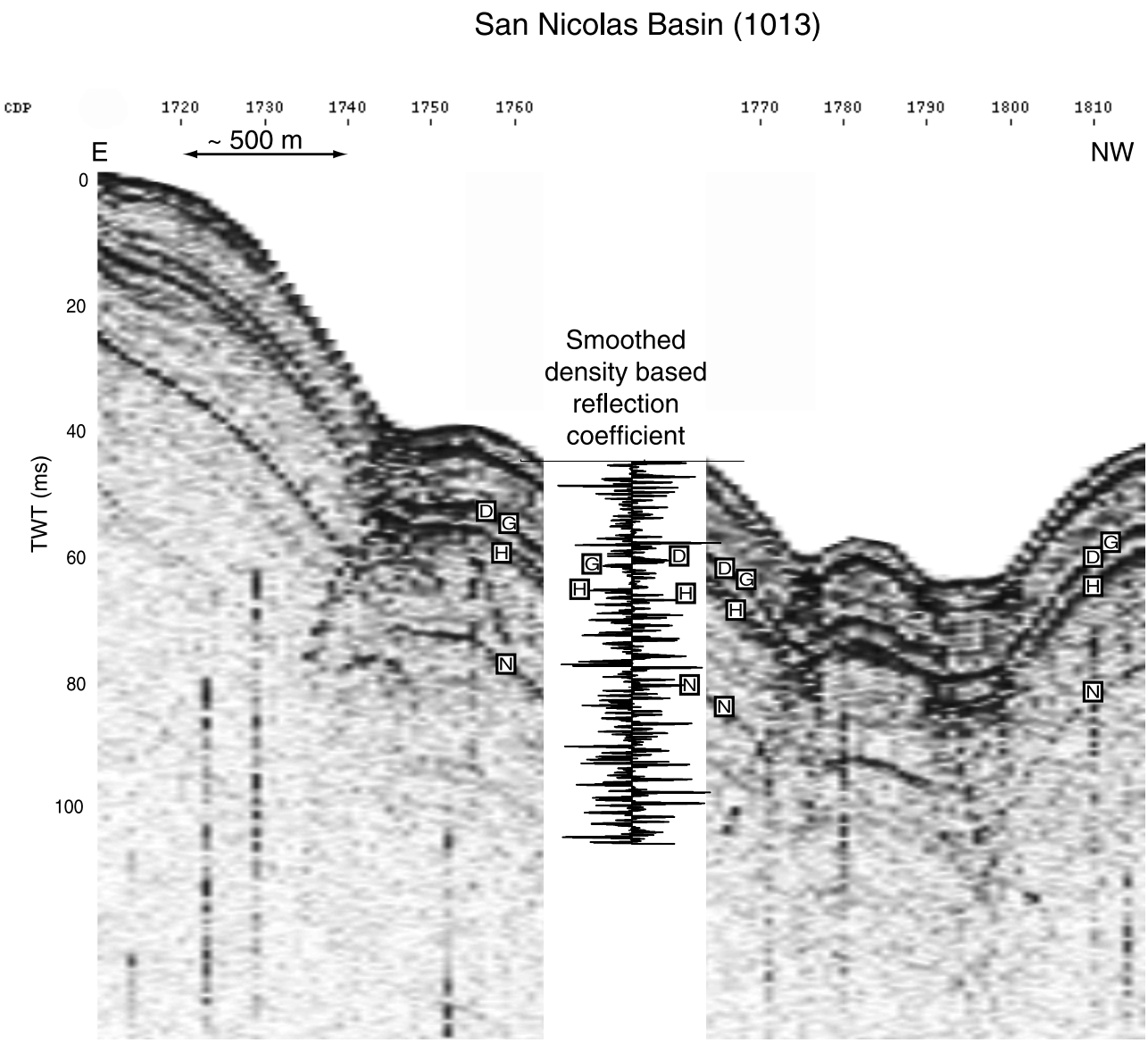

Figure 7. Correlation between the reflection coefficient and 3.5 kHz profile at Site 1013. The density was low-pass filtered (equivalent to 6 point smoothing). A velocity of 1500 m/s was used for approximate depth-to-time conversion. The reflection coefficient section represents 45 m of sediment.

and reduce the high frequency fluctuations resulting either from local variability or from noise in the GRAPE data (Figure 9).

[40] The smoothed density profiles (Figure 9b) reveal a remarkable similarity between the major concurrent density features at East Cortes (1012), San Nicolas (1013) and Tanner (1014) Basins. Geological processes leading to the formation of the bulk density profile must have been essentially the same in all those basins over the last 500 k.y. These common density features produce the reflectors in the 2–4 kHz frequency range, implying that at least some reflectors should be correlative in all three basins, and probably other outer Borderland basins as well. In Figures 9a and 9c the density and reflection coefficient profiles were plotted together with the interpreted seismic horizons superimposed in gray. The good correlation of the D-G-H reflector package and reflector N suggests that they are of regional character. At Site 1012, although no digital 3.5 kHz data were available, the regional nature of the reflectors is confirmed by density similarities. The reflectors were approximately dated (Table 5) using the combination of preliminary oxygen isotopes age models developed at Site 1012 [*Andreasen et al.*, 2000] and Site 1014 [*Hendy and Kennett*, 2000] (A. C. Ravelo, personal communication, 2000). The age values in Table 5 are presented as a range of values to account for error arising from lack of precise seismic velocity models that precluded accurate conversions from the depth domain to the seismic two way travel time.

[41] Reflectors D and G seem to be combined at Site 1013. At Site 1014 we have picked them as two separate seismic horizons. Horizons D and G at Site 1012 may be expressed as one horizon at the Marine Isotope

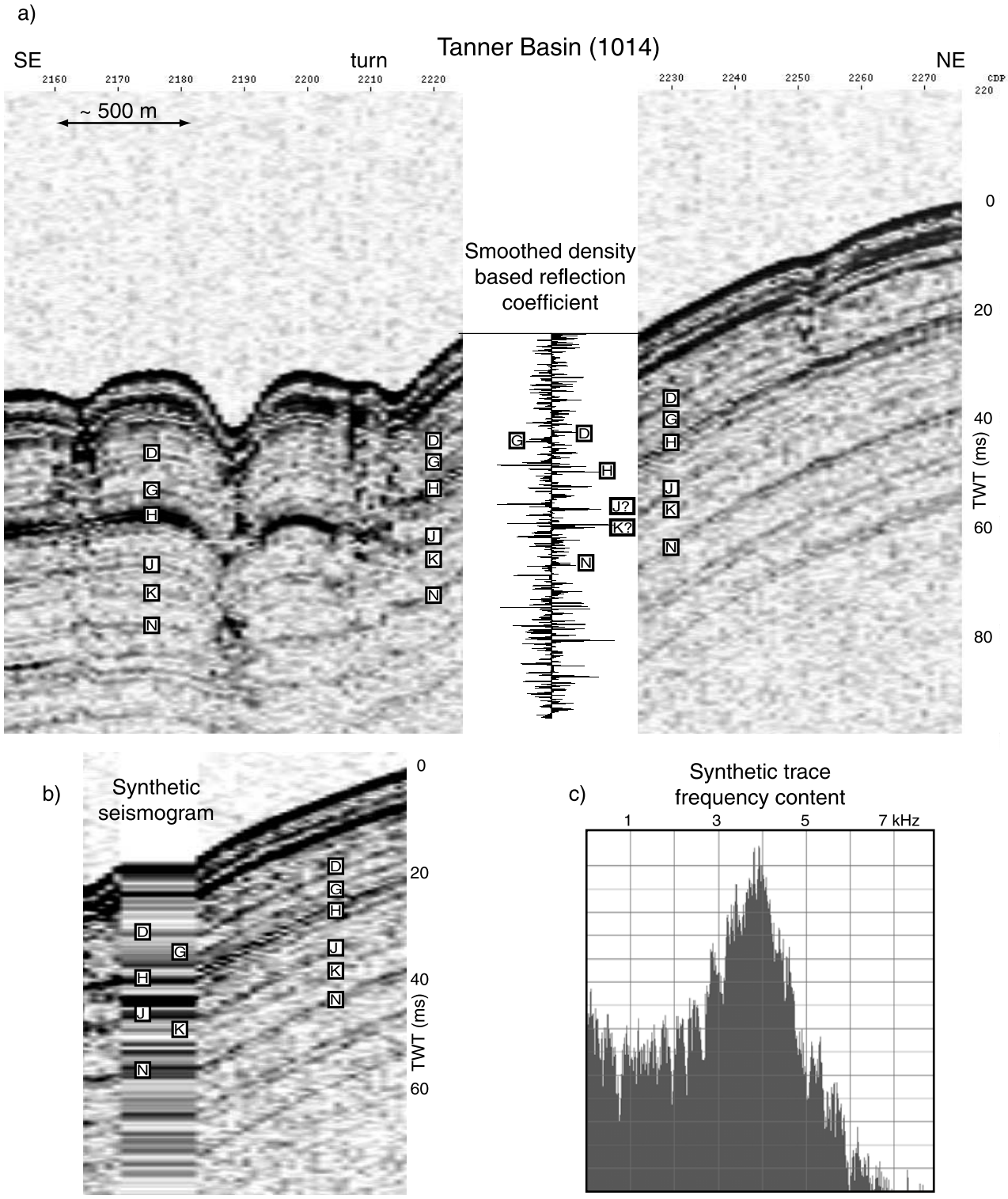

Figure 8. (a) Correlation between the reflection coefficient and 3.5 kHz profile at Site 1014. The density was low-pass filtered (equivalent to 6 point smoothing, 24 cm). A velocity of 1480 m/s was used for approximate depth-to-time conversion. The reflection coefficient section represents 52 m of sediment. (b) Synthetic seismogram at Site 1014. (c) The frequency content of the synthetic trace.

Stage (MIS) 5e. Horizon H may be missing at Site 1012 because there is no distinctive density gradient at the depth of 14–16 mbsf, where H would be anticipated based on the density correlation at the three sites. (Figure 9b).

[42] The regional character of some of the interpreted reflectors is further verified by investigations carried out earlier by Legg (M. Legg, personal communication, 2001) who noted well-defined reflections in the 3.5 kHz data in

Table 5. Approximate Ages of Correlatable Seismic Horizons of the Outer California Borderland Basins in the 2–5 kHz Frequency Range

Seismic Horizon	MIS	Approximate depth at Tanner Basin (1014)	Approximate depth at East Cortes Basin (1012)	Approximate age (ka)
D	5d–5e	12.95–13.47	11.39–12.07	115–123[a]
G	5e–6	14.63–15.11	12.95–13.23	129–133[a]
H	6	17.07–18.71	14.63–15.63(absent?)	145–175[a]
J?	7	23.19–24.03	19.67–20.31	224–237[b]
K?	8	25.71–26.27	21.99–22.59	257–267[b]
N	9–10	30.99–31.63	27.87–28.19	337–355[b]

[a]Age from *Hendy and Kennett* [2000].
[b]Age from A. C. Ravelo (personal communication, 2000).

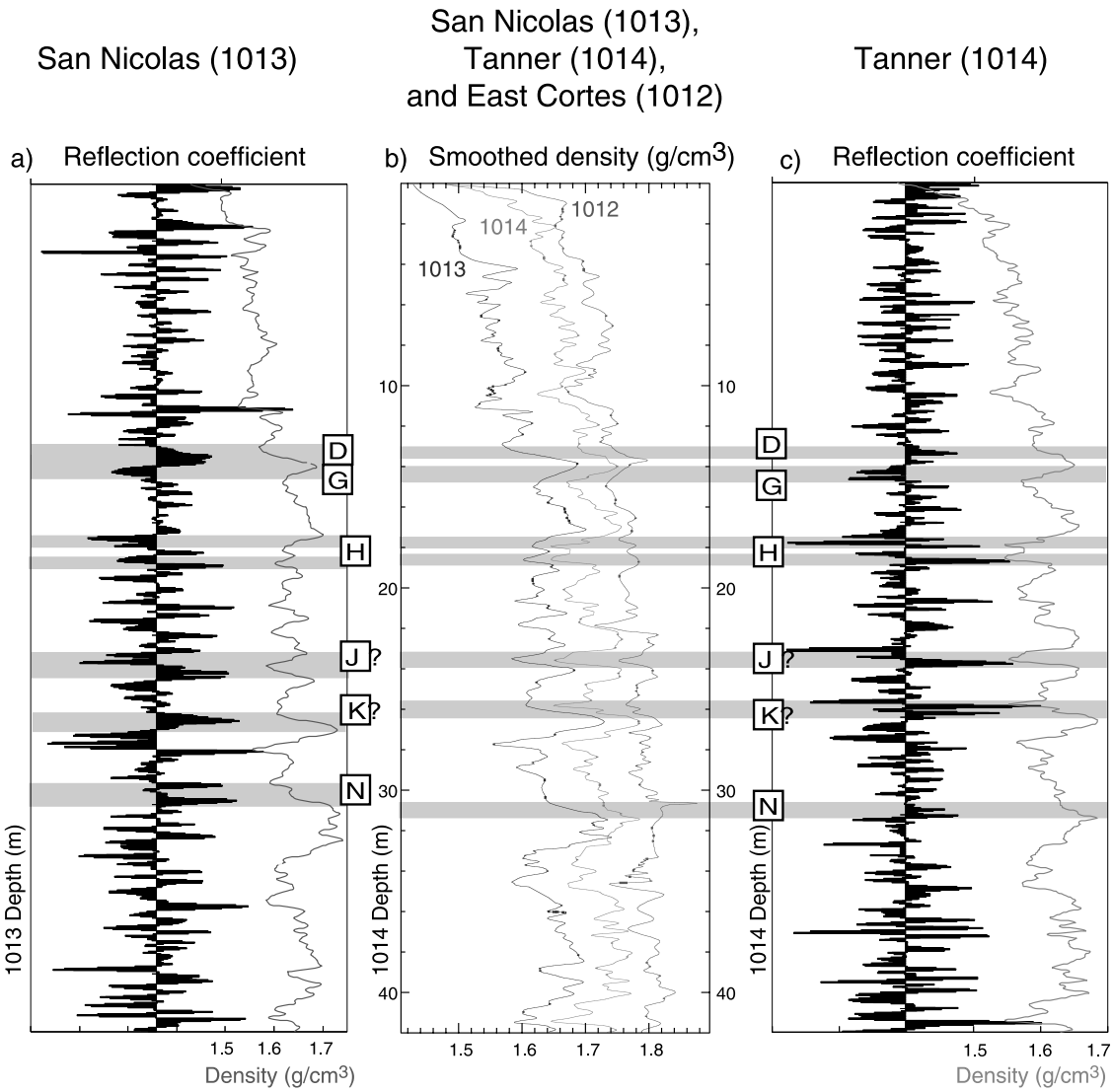

Figure 9. Density and reflection coefficient comparison for the 3 sites. (a) Smoothed density and reflection coefficient profile at Site 1013. Depth scale has been slightly linearly stretched, so 37 mbsf at Site 1013 corresponds to 42 mbsf at Site 1014. (b) Smoothed density profiles at Sites 1013, 1014 (plus 0.1 g/cm^3), and 1012 (plus 0.15 g/cm^3) plotted in an adjusted common depth scale (depth equivalent to Site 1014; depth of Site 1012 adjusted to depth of Site 1014 based on the correlation between stable oxygen isotope data at both sites). Blue, Site 1013; red, Site 1014; and green, Site 1012. (c) Smoothed density and reflection coefficient profile at Site 1014. Gray lines mark the interpreted seismic horizons from 3.5 kHz profiles. See color version of this figure at back of this issue.

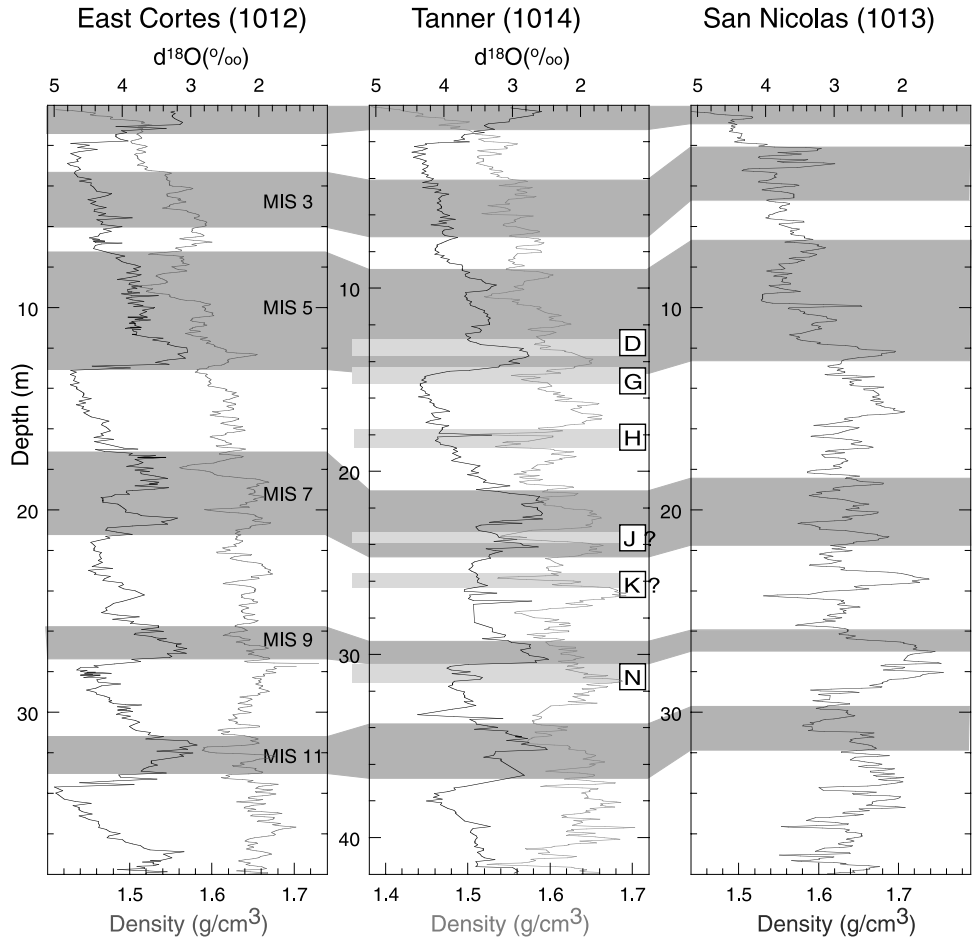

Figure 10. GRAPE density and oxygen isotope data at Sites 1012, 1014, and 1013 [*Hendy and Kennett*, 2000; *Andreasen et al.*, 2000] (A. C. Ravelo, personal communication, 2000). The Marine Isotope Stages (MIS) were marked according to *Imbrie et al.* [1984]. The shaded rectangles show the interpreted position of the reflectors on 3.5 kHz profiles. See color version of this figure at back of this issue.

North San Clemente basin that appeared to correlate with major highstands at Marine Isotope Stage 5e (possibly D-G) and 7 (possibly J).

6. Origin of Fine-Scale Density Fluctuations and the Cause of Seismic Reflections

[43] The regionally similar density patterns and seismic horizons in the Pleistocene sequences of the outer Borderland basins must reflect common paleoprocesses. We review pertinent studies from other parts of the Pacific.

6.1. Seismic Stratigraphy in Other Parts of the Pacific

[44] There is a large volume of literature connecting seismic reflections and their inferred causative agents in various regions of Pacific Ocean. For example, *Mosher et al.* [1993] inferred that seismic reflections on 80 in^3 watergun profiles from the deep-water carbonate Ontong Java Plateau derive at least partly from grain-size fluctuations. *Jarrard and Symonds* [1993] showed that within carbonate sediments along the NE Australian margin, the acoustic impedance responds directly to porosity in studied sediments and indirectly to lithology and diagenetic processes.

[45] In the central equatorial Pacific, also influenced by upwelling-driven processes, *Mayer et al.* [1985] suggested that major sedimentary reflectors observed on 80 in^3 watergun seismic profiles are related to carbonate variations or diagenetic events. In this setting, sediments are primarily a two component system consisting of calcium carbonate and biogenic opal, with very minimal amounts of clay. Carbonate variation caused a variable density profile, which in turn produced characteristic seismic reflection profiles. *Bloomer et al.* [1995] showed that in the eastern equatorial Pacific major reflectors observed on 80 in^3 watergun seismic profiles were also caused by sharp changes in bulk density related to variations in the carbonate content. The relationship between calcium carbonate content and bulk density in the equatorial Pacific is so strong that density can be utilized for carbonate predictions in paleoclimate studies [*Mayer*, 1991]. Acoustic properties of equatorial Pacific sediments change directly in response to the changes in carbonate content and thus ocean chemistry. Hence, the seismic record from the equatorial Pacific potentially could be viewed as a record of changing paleoceanographic conditions.

[46] In contrast to the carbonate equatorial Pacific deposits, the California Borderland sedimentary components include clays, carbonates, organic carbon and minor

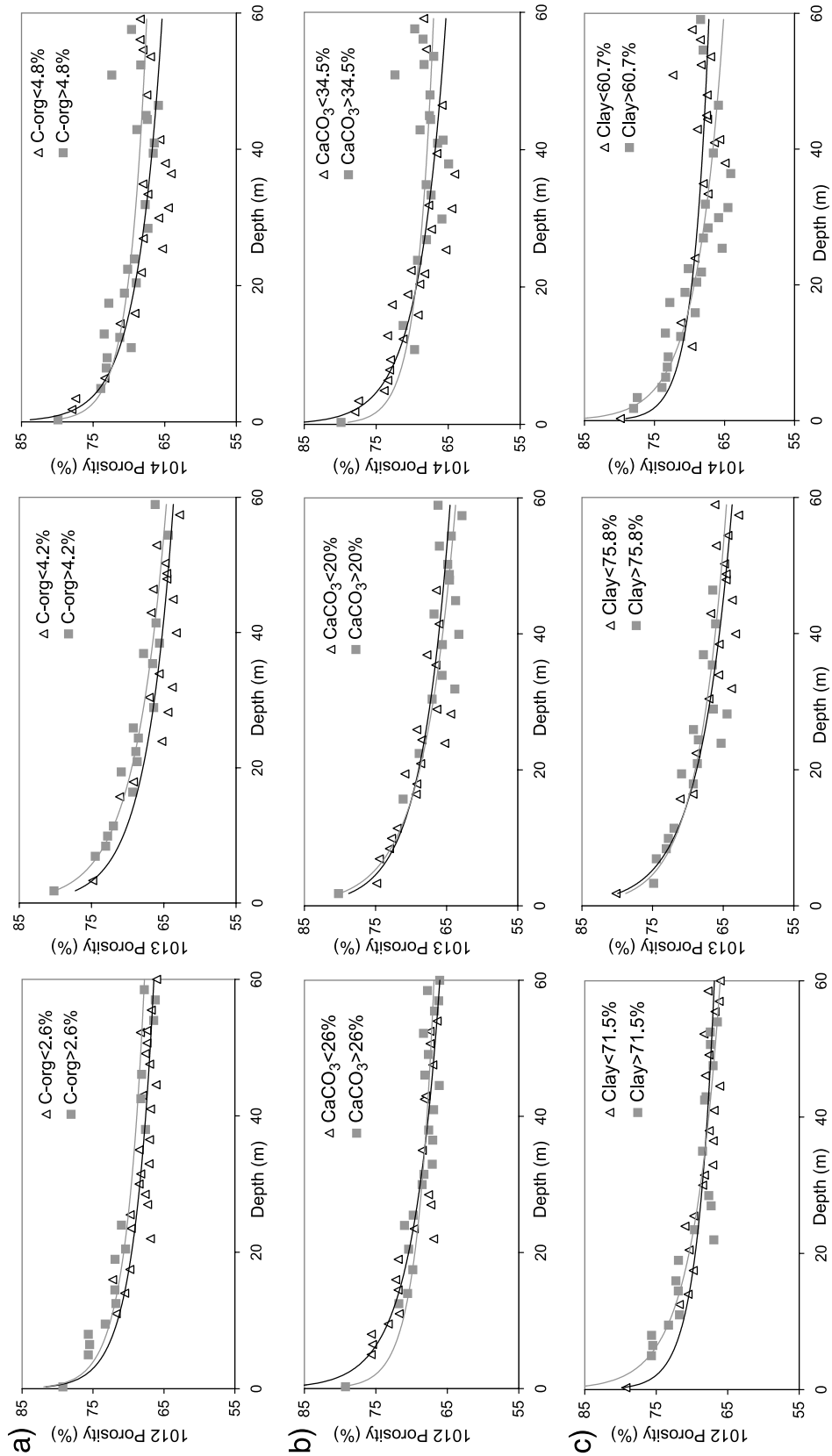
a)
b)
c)
1012 Porosity (%)
1013 Porosity (%)
1014 Porosity (%)
Depth (m)
C-org<2.6%
C-org>2.6%
C-org<4.2%
C-org>4.2%
C-org<4.8%
C-org>4.8%
CaCO3<26%
CaCO3>26%
CaCO3<20%
CaCO3>20%
CaCO3<34.5%
CaCO3>34.5%
Clay<71.5%
Clay>71.5%
Clay<75.8%
Clay>75.8%
Clay<60.7%
Clay>60.7%

Figure 11

Table 6. Results of ANCOVA (Analysis of Covariance) and *F* Test to Examine if the Hypothesis That the Regression Slopes are the Same (e.g., Samples With Modest Differences in Lithology Follow the Same Compaction Trend) can be Rejected

Site	Property	*F* Computed	*F* From the Table [*Neter et al.*, 1996]	*F* Test	Probability, P	Slopes
1012	$CaCO_3$	F_c (0.05, 1, 34) = 2.314	F (0.05,1,30) = 4.17	$F_c < F$	0.137	same[a]
	C-org	F_c (0.05, 1, 35) = 3.859	F (0.05,1,30) = 4.17	$F_c < F$	0.057	same[a]
	Clay	F_c (0.05, 1, 35) = 2.136	F (0.05, 1, 30) = 4.17	$F_c < F$	0.153	same[a]
1013	$CaCO_3$	F_c (0.05, 1, 39) = 7.269	F (0.05, 1, 30) = 4.17	$F_c > F$	0.038	different
	C-org	F_c (0.05, 1, 31) = 0.802	F (0.05, 1, 30) = 4.17	$F_c < F$	0.377	same[a]
	Clay	F_c (0.05, 1, 31) = 0.744	F (0.05, 1, 30) = 4.17	$F_c < F$	0.395	same[a]
1014	$CaCO_3$	F_c (0.05, 1, 39) = 7.269	F (0.05, 1, 30) = 4.17	$F_c > F$	0.010	different
	C-org	F_c (0.05, 1, 39) = 3.681	F (0.05, 1, 30) = 4.17	$F_c < F$	0.062	same[a]
	Clay	F_c (0.05, 1, 39) = 8.498	F (0.05, 1, 30) = 4.17	$F_c > F$	0.006	different

[a]There is not enough statistical evidence to reject the hypothesis that the slopes are different, so for the purpose of this study, we consider them equal.

amounts of opal. Nevertheless, the results from the equatorial Pacific suggest that the answer to our original question resides in how density changes as a function of sediment composition.

6.2. Effect of Compaction on Density

[47] In order to examine bulk density variations caused by compositional changes alone, compaction must be removed. Various compaction mechanisms have been proposed, which all depend on one or more of the following variables: sediment type, the amount of pressure, and the time involved [e.g., *Baldwin and Butler*, 1985; *Schon*, 1996]. To evaluate sediment compaction behavior under burial pressure in California Borderland basins, we examined porosity variations with depth for the upper 60 m for samples with different compositions from Sites 1012, 1013, and 1014 (Figure 11). Logarithmic curves were fitted to the porosity-depth profiles for samples with different compositions. It can be observed that the fitted curves essentially overlap within the margin of error of porosity and composition measurements [*Lyle et al.*, 1997], indicating that the trend in porosity decrease with depth in the upper 60 mbsf is to the first order independent of lithology.

[48] To further validate this conclusion we performed statistical tests to find out if there is enough evidence to reject the hypothesis that samples of moderately different composition follow the same compaction trend. Prior to carrying out the regressions and analysis of covariance (ANCOVA), the curves in Figure 11 had to be linearized and for that purpose the natural logarithm transformation of the independent variable (depth) was chosen. Subsequently, covariance analyses were performed to test the significance of the difference in slopes for the two regression lines representing samples with different composition. Traditionally, experimenters use either the 0.05 level (sometimes called the 5% level) or the 0.01 level (1% level), although the choice of levels is largely subjective. For this study we used 5% (95% confidence interval). The calculations were completed for all 9 cases and the final results are assembled in Table 6.

[49] Two out of three cases that gave enough statistical evidence to reject the hypothesis in Table 6 were those with different calcium carbonate and clay contents at Site 1014. This could be explained by the fact that at Site 1014 there is larger sample variance in, for example, the $CaCO_3$ content (145.7) than at Sites 1012 (141) and 1013 (88). For all other six cases the analysis of covariance (ANCOVA) confirms that the slopes can be considered the same. This suggests that compaction of sediments in the California Borderland in the upper 60 mbsf is largely independent of modest differences in lithology. This result is expected considering the soft consistency of the sediments and relatively low overburden pressures corresponding to 60 mbsf. In such cases, the initial cause of compaction is expulsion of water and the sliding of loosely-constrained particles into more stable positions [*Schopper*, 1982]. The general increase of density with depth for the upper 60 mbsf is therefore due to decreases in the relatively high porosities and is independent of the moderate changes in the bulk composition of the sediments.

[50] The sediment behavior may be different in the surface layer (0–1 m), but we have not included this interval. The compaction analyses were started at a depth of about 1 mbsf, where the first samples for gravimetric porosity measurements were taken to avoid the very top of the first APC cores, as they are usually somewhat disturbed and/or compressed. It is within these upper few centimeters where the most dramatic physical and chemical changes occur at the seawater-sediment interface [*Bennett et al.*, 1999]. Studies here are important for understanding early digenesis and to understand the reflection from the seafloor but they are not crucial for prediction of the larger scale compaction trend.

[51] To remove the compaction effect from density at Site 1012, the logarithmic curve y (2) was fitted to the density profile (Figure 12) and for each depth d the trend y was subtracted from the density value to obtain detrended density or ''density before compaction'' (called later decompacted density):

$$y = 0.0416 * \ln(d) + 1.4959. \quad (2)$$

[52] Site 1012 was chosen for these analyses because high resolution geochemical measurements were collected only at that site, and the good correlation between the

Figure 11. Depth-porosity profiles for top 60 m of Sites 1012, 1013, and 1014 for samples with different chemical composition. (a) Different organic carbon content. (b) Different calcium carbonate content. (c) Different clay content. Logarithmic curves fitted to the porosity-depth profiles for the different samples almost overlap, indicating that compaction of sediments in the California Borderland in the top 60 m is largely independent of modest differences in lithology.

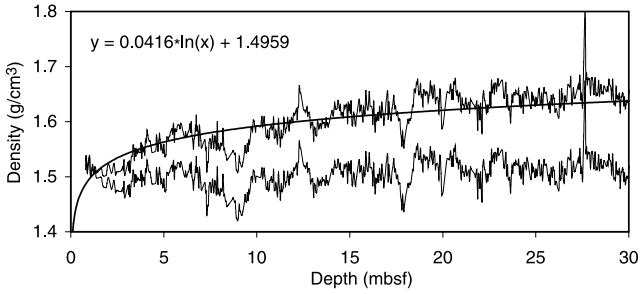

Figure 12. Removal of the compaction trend from the density data at Site 1012. Density profile is fitted with logarithmic curve representing the compaction trend. The trend is subtracted from the density profile. Resulting leveled curve represents the density without the compaction trend.

density at the three sites allows us to confidently extrapolate any interpretations from Site 1012 to Sites 1013 and 1014.

[53] To calculate the decompacted density we used the high resolution (4 cm sampling interval) GRAPE density data. In the next step the decompacted density profile is compared with lithology to verify how density variations causing the regional seismic reflections on 3.5 kHz profiles relate to compositional changes.

6.3. Correlation of Decompacted Density With Geochemical Data

[54] The decompacted bulk densities vary only as a function of the composition of the sediments because the overburden pressure dependency has been removed. To investigate the compositional variations that generate the density fluctuations, the detrended density profiles were plotted against organic carbon (Figure 13a) and calcium carbonate contents (Figure 13b). This comparison shows a very close relationship between bulk density and organic carbon content (inverse relationship) and a relatively poor correspondence between density and calcium carbonate. The explanation of such a good correlation between organic matter content and bulk density lies in the proportion of different components that comprise the sediments and the mutual relationships between their grain densities. Pleistocene sediments in the three cored basins of the outer California Borderland are characterized by high organic carbon concentrations, ranging between 1 and 7 weight percent (Figure 14). The grain density of organic carbon is less than 1.5 g/cm^3, so it is much lower than the density of the background clay rich sediments (2.6 g/cm^3) and of $CaCO_3$ (2.71 g/cm^3). Hence, a small increase or decrease in C-org affects bulk density more than the same weight percent change of $CaCO_3$ or clay.

[55] This inverse relationship between density and organic carbon indicates that the acoustic characteristics of Borderland sediments are markedly different from equatorial Pacific deposits [*Mayer*, 1991], where the controlling factor for density is the calcium carbonate content.

[56] We earlier established that density variations correspond well to the reflectors on 3.5 kHz seismic profiles. We have shown now that these density fluctuations correlate with changes in organic carbon content. These observations

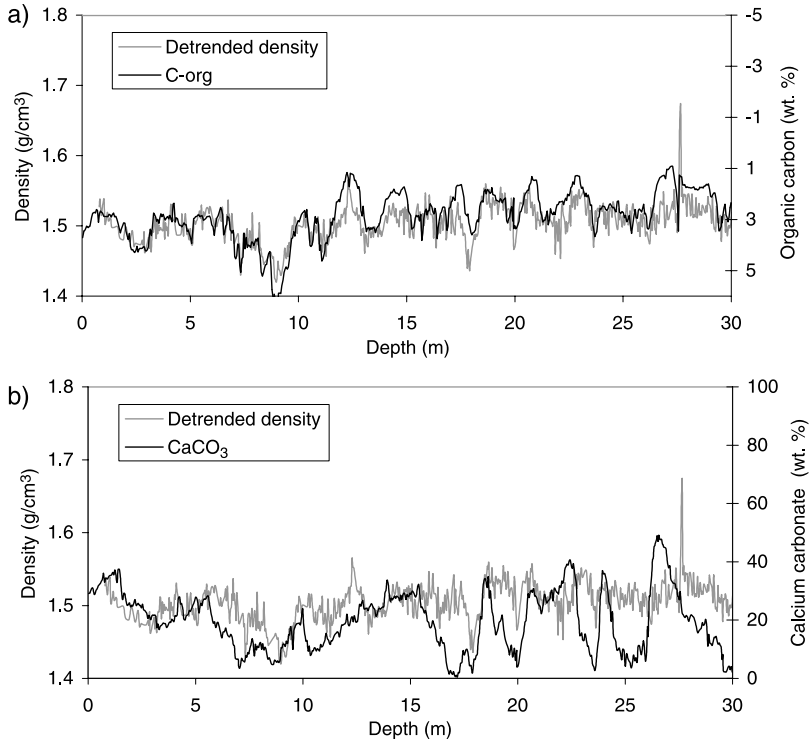

Figure 13. Evaluation of the relationship between the decompacted density chemical composition. (a) Comparison between the decompacted density and organic carbon. The two curves show a close resemblance. (b) Comparison between the decompacted density and calcium carbonate content. The correlation is weak at best.

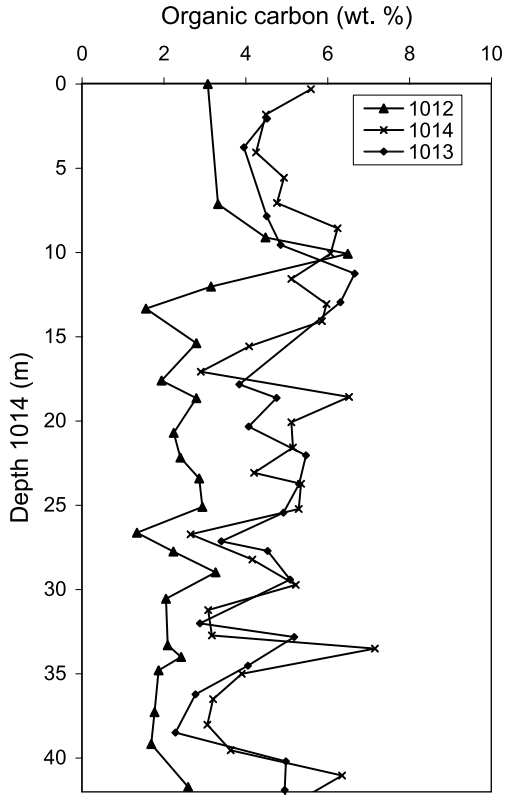

Figure 14. Shipboard organic carbon measurements at Sites 1012, 1013, and 1014 plotted at the common adjusted depth scale (equivalent to the depth of Site 1014).

together indicate that variations in organic matter content presumably account for seismic reflections in the outer California Borderland basins in the 2–4 kHz frequency range. This is a significant discovery since there apparently is no other paleoceanographic setting that we know of where such a close linkage between acoustic properties and organic carbon has been established.

6.4. Paleoceanographic Importance

[57] Organic carbon accumulation results from the interplay between organic matter influx to the seafloor from both high primary marine productivity and terrigenous sources, and the preservation rate, which is related to oxygen content in the water column. To distinguish between the marine and terrestrial origins of organic matter, the ratio of total organic carbon to total nitrogen is routinely measured [*Bordovskiy*, 1965; *Emerson and Hedges*, 1988]. Such measurements performed on the outer California Borderland sediments suggest a marine provenance of the Pleistocene organic matter [*Lyle et al.*, 1997], with only episodic input of terrigenous material. A mostly marine origin for the organic carbon indicates that paleoceanographic conditions in the region rather than terrigenous input were responsible for its accumulation and abundance. The key paleoceanographic feature of the Borderland basins responsible for high primary productivity is upwelling. The outer basins all lie under the influence of the same major eddy in the California Current upwelling system. This would explain the strong similarity in the records of density and organic carbon deposition in these basins and the resulting regional reflectors. The small differences in the organic carbon content at the three basins might be attributed to slight changes in terrigenous dilution or to a somewhat different preservation regime in the three basins. Lower organic carbon contents in the East Cortes Basin (Figure 14) in comparison to the Tanner and San Nicolas Basins perhaps can be attributed to the basins' locations with respect to the oxygen minimum depth. The sills of the San Nicolas and Tanner Basins are located closer to the core of the oxygen minimum zone (Figure 15) and consequently have higher organic carbon preservation rates due to oxygen depletion, whereas the East Cortes Basin, which is situated deeper below the oxygen minimum, has lower organic carbon contents due to more oxygenated waters.

6.5. Neotectonic Significance

[58] The dated regional reflectors identified in the outer California Borderland basins have application for neotectonic studies aimed at understanding earthquake hazards in California. To accurately assess the earthquake hazard to coastal southern California, the potential for large earthquakes on the major offshore faults must be determined. The San Clemente and San Diego Trough fault zones are two examples of long and well defined inner borderland fault zones. Based on multibeam bathymetry, high-resolution seismic data and submersible Alvin observations [*Goldfinger et al.*, 2000], both of these structures rupture the seafloor in actively sedimented basins and are therefore probably active themselves.

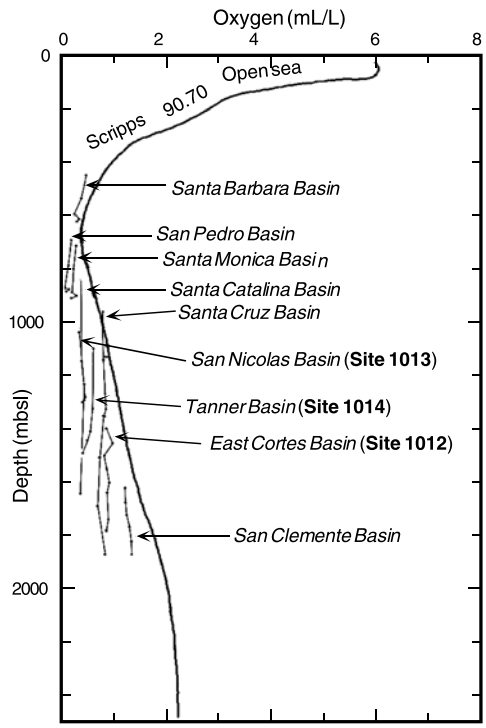

Figure 15. Oxygen profiles within each California Borderland basin [from *Emery*, 1960]. As a rule, the oxygen content in benthic waters from each basin is inherited from the open ocean. Basins with sills near the oxygen minimum have significantly less dissolved oxygen than deeper basins.

[59] The correlative seismic horizons in the outer California Borderland basins provide an age model for sediments that can be measured remotely. Because of the regional character of the horizons they can be probably tied to the sediments offset by the San Clemente fault. As a result, it should be possible to model the vertical uplift of these dated horizons where they are involved in restraining bend uplifts of known geometry. The modeled vertical deformation will allow constraints to be placed on the horizontal slip rate, which would otherwise not be possible using horizontal reflectors offset by strike-slip faulting.

7. Conclusions

[60] 1. We have developed a simple processing scheme for digitally-recorded 3.5 kHz data that greatly increases the signal-to-noise ratio and improves the coherency of the seismic horizons without affecting the amplitudes. The procedure includes removal of the heave noise by horizon flattening and smoothing followed by reflection strength display.

[61] 2. The 3.5 kHz data with sub meter resolution are of approximately the scale needed to study the Pleistocene sedimentary features in this area.

[62] 3. Within the top 50 m of the studied Borderland sediment sequence, sediment bulk density controls the acoustic impedance. This study confirms previous observations from the equatorial Pacific, where the density of the unconsolidated sediments also exerted the major influence on acoustic properties in a distinctly different sedimentary environment. Reflection coefficient profiles constructed based on smoothed sediment bulk density correspond well to major horizons on 3.5 kHz images, even though a simple model with constant velocity was used to obtain the depth-to-time (TWT) conversion.

[63] 4. Strong resemblance between concurrent features on the smoothed density profiles from the three outer basins indicates that there is a common sedimentation pattern throughout the Pleistocene in these basins. Density similarities result in acoustic impedance similarities, and consequently some reflectors can be correlated from basin to basin or predicted to be correlated. This creates the possibility of using the identified reflectors as chronostratigraphic markers for other outer basins that have not yet been drilled, but for which have 3.5 kHz profiles are available.

[64] These regional seismic horizons represent changes in sediment properties resulting from major global climatic transitions and events and can be correlated with Marine Isotope Stages and stage boundaries.

[65] Assigning a preliminary age to the identified reflectors is important not only from a paleoceanographic standpoint, but also could benefit tectonic studies of the Borderland. The dated regional Borderland horizons may provide an aid in determining the rates of tectonic activity along the adjacent Borderland offshore faults (e.g., San Clemente fault zone).

[66] 5. Density fluctuations corrected for compaction inversely correlate with marine organic carbon content and do not correlate with calcium carbonate content. Such a good match between organic carbon-driven density fluctuations and horizons on 3.5 kHz profiles leads to the conclusion that seismic reflections in the California Borderland over the last 0.5 Ma are related to variations in the organic carbon content of the sediments. A marine provenance of the organic carbon indicates that its fluctuations are related to paleoceanographic rather than tectonic variations.

[67] This is the first location we know of where variations in organic carbon content determine seismic reflectors. A very important implication of good correlation between the impedance and organic carbon is the potential for estimation of composition from seismic data if a better source signature and velocity were available.

[68] **Acknowledgments.** Many thanks to Anne Trehu, John Townend, and an anonymous reviewer for very helpful reviews of the manuscript. We would also like to express our gratitude to Gregor Eberli, Bruce Rosendahl, Chris Goldfinger, Chris Sorlien, Mark Legg, and Uri ten Brink for their very valuable comments and discussions. Finally, we thank Kimberly Rosen and Helena Molina for their assistance with various aspects of the manuscript. This research used samples and data provided by the Ocean Drilling Program (ODP). The ODP is sponsored by the U.S. National Science Foundation (NSF) and participating countries under management of Joint Oceanographic Institutions (JOI), Inc. Funding for this research was provided by the U.S. Science Support Program. We thank the officers and crew of the R/V *Maurice Ewing* for their assistance in collecting the seismic data during cruise EW9709 (digital 3.5 kHz--grant NSF OCE-9634141) and EW9504 (80 ci seismic reflection). MWL was also partially supported by the NSF-Idaho EPSCoR Program and by the National Science Foundation under award numbers EPS-0132626 and OCE-9907292.

References

Andreasen, D. H., M. Flower, M. Harvey, S. Chang, and A. C. Ravelo (2000), Data Report: Late Pleistocene oxygen and carbon isotopic records from sites 1011, 1012, and 1018, *Proc. Ocean Drill. Program, Sci. Results*, *167*, 141–144.

Atwater, T. (1989), Plate tectonic history of the Northeast Pacific and western North America, in *The Eastern Pacific Ocean and Hawaii*, edited by E. Winterer, D. Hussong, and R. Decker, pp. 21–72, Geol. Soc. of North Am., Boulder, Colo.

Baldwin, B., and C. O. Butler (1985), Compaction curves, *AAPG Bull.*, *69*(4), 622–626.

Behl, R. J., and J. P. Kennett (1996), Brief interstadials events in Santa Barbara Basin, Northeast Pacific, during the past 60 k.y., *Nature*, *379*, 243–246.

Bennett, R. H., B. Ransom, M. Kastner, R. J. Baerwald, M. H. Hulbert, W. B. Sawyer, H. W. Olsen, and M. W. Lambert (1999), Early diagenesis impact of organic matter on mass physical properties and processes, California continental margin, *Mar. Geol.*, *159*, 7–34.

Biot, M. A. (1956a), Theory of propagation of elastic waves in a fluid-saturated porous solid. I. Low-frequency range, *J. Acoust. Soc. Am.*, *28*, 168–178.

Biot, M. A. (1956b), Theory of propagation of elastic waves in a fluid saturated porous solid. II. Higher frequency range, *J. Acoust. Soc. Am.*, *28*, 179–191.

Bloomer, S., L. Mayer, and T. Moore (1995), Seismic stratigraphy of the eastern equatorial Pacific Ocean: Paleoceanographic implications, *Proc. ODP Sci. Results*, *138*, 537–553.

Bodine, J. H. (1984), Waveform analysis with seismic attributes, *Oil and Gas J.*, *84*(24), 59–63.

Bohannon, R. G., and E. Geist (1998), Upper crustal structure and Neogene tectonic development of the California continental borderland, *Geol. Soc. Am. Bull.*, *110*(6), 779–800.

Bohannon, R. G., and T. Parsons (1995), Tectonic implications of post-30 Ma Pacific and North American relative plate motions, *Geol. Soc. Am. Bull.*, *107*(8), 937–959.

Bordovskiy, O. K. (1965), Accumulation and transformation of organic substances in marine sediment, Sources of organic matter in marine basins, *Mar. Geol.*, *3*, 5–31.

Boyce, R. (1976), Definitions and laboratory techniques of compressional velocity parameters and wet-water content, wet-bulk density, and porosity parameters by gravimetric and gamma ray attenuation techniques, *Initial. Rep. Deep Sea Drill. Proj.*, *33*, 931–958.

Brocher, T. M., R. W. Clayton, K. D. Klitgord, R. G. Bohannon, R. Sliter, J. K. McRaney, J. V. Gardner, and J. B. Keene (1995), LARSE: Multi-

channel Seismic Reflection Profiling on the R/V *Maurice Ewing* During the Los Angeles Region Seismic Experiment, California, *Open-File Rep. 95–228*, U. S. Geol. Surv., Menlo Park, Calif.

Brown, A. (1999), Interpretation of three-dimensional seismic data, in *AAPG Memoir 42*, *SEG Invest. in Geophys.*, vol. 9, AAPG, Prague, Czech Republic.

Bull, D., and A. Kemp (1996), Composition and origins of laminae in late Quaternary and Holocene sediments from the Santa Barbara Basin, in *Palaeoclimatology and Paleoceanography from Laminated Sediments*, edited by A. Kemp, *Geol. Soc. Spec. Publ.*, *116*, 143–156.

Chen, Q., and S. Sidney (1997), Seismic attribute technology for reservoir forecasting and monitoring, *Leading Edge*, *16*(5), 445–456.

Crouch, J. K., and J. Suppe (1993), Late Cenozoic tectonic evolution of the Los Angeles basin and inner California borderland: A model for core-complex like extension, *Geol. Soc. Am. Bull.*, *105*, 1415–1434.

Dixon, T. H., F. Farina, C. DeMets, F. Suarez-Vidal, J. Fletcher, B. Marquez-Azua, M. Miller, O. Sanchez, and P. Umhoefer (2000), New kinematic models for Pacific-North America motion from 3 Ma to present, II: Evidence for a "Baja California shear zone," *Geophys. Res. Lett.*, *27*, 3961–3964.

Dunkel, C. (2001), Oil and Gas Resources in the Pacific Outer Continental Shelf as of January 1, 1999, *OCS Report MMS*, *2001–014*, pp. 1–16, Mineral Manage. Serv., Pac. OCS Region, U.S. Dept. of the Int., Washington, D. C.

Emerson, S., and J. I. Hedges (1988), Processes controlling the organic carbon content of open ocean sediments, *Paleoceanography*, *3*, 621–634.

Emery, K. O. (1960), *The Sea off Southern California*, John Wiley, Hoboken, N. J.

Feigl, K. L., et al. (1993), Space geodetic measurement of crustal deformation in central and southern California, 1984–1992, *J. Geophys. Res.*, *98*, 21,677–21,712.

Goldfinger, C., M. Legg, and M. Torres (2000), New mapping and submersible observations of recent activity of the San Clemente fault, *Eos Trans. AGU*, *81*(48), Fall Meet. Suppl, Abstract 1069.

Gorsline, D., and L. Teng (1989), The California continental borderland, in *The Eastern Pacific Ocean and Hawaii*, edited by E. Winterer, D. Hussong, and R. Decker, pp. 471–487, Geol. Soc. of North Am., Boulder, Colo.

Gorsline, D. S., D. E. Drake, and P. W. Barnes (1968), Holocene sedimentation in Tanner Basin, California Continental Borderland, *Geol. Soc. Bull.*, *79*, 659–674.

Gorsline, D., E. Nava-Sanchez, and J. Murillo de Nava (1996), A survey of occurrences of Holocene laminated sediments in California Borderland basins: Product of a variety of depositional processes, in *Palaeoclimatology and Paleoceanography from Laminated Sediments*, edited by A. Kemp, *Geol. Soc. Spec. Publ.*, *116*, 93–110.

Gumacher, C., W. R. Normark, S. L. Ross, B. D. Edwards, R. Sliter, P. Hart, B. Cooper, J. Childs, and J. A. Reid (2000), Cruise Report for A1-00-SC, Southern California Earthquake Hazards Project, Part A, *Open-File Rep. 00–516*, U. S. Geol. Surv., Menlo Park, Calif.

Hamilton, E., and T. Bachman (1982), Sound velocity and related properties of marine sediments, *J. Acoust. Soc. Am.*, *72*(6), 1891–1904.

Hendy, I. L., and J. P. Kennett (2000), Stable isotope stratigraphy and paleoceanography of the last 170 k.y.: Site 1014, Tanner Basin, California, *Proc. Ocean Drill. Program Sci. Results*, *167*, 129–140.

Herbert, T. D., J. D. Schuffert, D. Andreasen, L. Heusser, M. Lyle, A. Mix, A. C. Ravelo, L. D. Stott, and J. C. Herguera (2001), Collapse of the California current during glacial maxima linked to climate change on land, *Science*, *293*, 71–76.

Huyer, A. (1983), Coastal upwelling in the California Current system, *Prog. Oceanogr.*, *12*, 259–284.

Imbrie, J., J. D. Hays, D. G. Martinson, A. McIntyre, A. C. Mix, J. J. Morley, N. G. Pisias, W. L. Prell, and N. J. Shackleton (1984), The orbital theory of Pleistocene climate: Support from a revised chronology of the marine ^{18}O record, in *Milankovitch and Climate: Understanding the Response to Astronomical Forcing*, part 1, edited by A. Berger et al., pp. 269–305, D. Reidel, Norwell, Mass.

Janecek, T. (2000), Late Neogene biogenic opal data for Leg 167 sites on the California margin, *Proc. Ocean Drill. Program, Sci. Results*, *167*, 213–214.

Jarrard, R., and P. Symonds (1993), Origin of seismic reflectors within carbonate-rich sediments from northeastern Australian margin, *Proc. ODP Sci. Results*, *133*, 649–659.

Legg, M. R. (1991), Developments in understanding the tectonic evolution of the California Continental Borderland, *Soc. Sedim. Geol. Spec. Publ.*, *46*, 291–312.

Legg, M., V. Wong, and F. Suarez (1991), Geologic structure and tectonics of the Inner Continental Borderland of Northern Baja California, in *The Gulf and Peninsular Province of the California*, edited by P. Dauphin and B. Simoneit, *AAPG Mem.*, *47*, 145–177.

Leurer, K. C. (1997), Attenuation in fine-grained marine sediments: Extension of the Biot-Stoll model by the "effective grain model" (EGM), *Geophysics*, *62*(5), 1465–1479.

Lyle, M., P. Gallaway, L. Liberty, A. Mix, L. Stott, D. Hammond, J. Gardner, W. Dean, and EW9504 Scientific Party (1995), W9406 and EW9504 Site Surveys of the California Margin proposed drilled sites, Leg 167, volume 2, *Seismic Profiles*, *Tech. Rep. BSU CGISS, 95–11*.

Lyle, M., I. Koizumi, C. Richter, and the Shipboard Scientific Party (1997), *Proceedings of the Ocean Drilling Program, Initial Reports*, vol. 167, Ocean Drill. Program, College Station, Tex.

Lyle, M., I. Koizumi, C. Richter, and T. C. Moore Jr. (2000), *Proceedings of the Ocean Drilling Program, Scientific Results*, vol. 167, Ocean Drill. Program, College Station, Tex.

Lynn, R. J., and J. J. Simpson (1987), The California Current system: The seasonal variability of its physical characteristics, *J. Geophys. Res.*, *92*, 12,947–12,966.

Marsaglia, K. M., K. C. Rimkus, and R. J. Behl (1995), Provenance of sand deposited in the Santa Barbara Basin at Site 893 during the last 155,000 years, *Proc. Ocean Drill. Program Sci. Results*, *146*, 61–75.

Mayer, L. (1991), Extraction of high-resolution carbonate data for palaeoclimate reconstruction, *Nature*, *352*, 148–150.

Mayer, L., T. Shipley, F. Theyer, R. Wilkens, and E. Winterer (1985), Seismic modeling and paleoceanography at Deep Sea Drilling Project Site 574, *Initial Rep. Deep Sea Drill. Proj.*, *85*, 947–970.

Miller, K. (2002), Geophysical evidence for Miocene extension and mafic magmatic addition in the California Continental Borderland, *Geol. Soc. Am. Bull.*, *114*(4), 497–512.

Mortyn, P. G., R. C. Thunell, D. M. Anderson, L. D. Scott, and J. Le (1996), Sea surface temperature changes in the Southern California Borderland during the last glacial-interglacial cycle, *Paleoceanography*, *11*, 415–430.

Mosher, D., and P. Simpkin (1999), Status and trends of marine high-resolution seismic reflection profiling - data acquisition, *Geosci. Can.*, *26*(4), 174–188.

Mosher, D., L. Mayer, T. Shipley, E. Winterer, R. Hagen, J. Marsters, F. Bassinot, R. Wilkens, and M. Lyle (1993), Seismic stratigraphy of the Ontong Java Plateau, *Proc. Ocean Drill. Program Sci. Results*, *130*, 33–49.

Murphy, W. F., K. W. Winkler, and R. L. Kleinberg (1986), Acoustic relaxation in sedimentary rocks: Dependence on fluid saturation, *Geophysics*, *51*, 757–766.

Neter, J., M. H. Kutner, C. J. Nachtsheim, and W. Wasserman (1996), *Applied Linear Statistical Models*, Richard D. Irwin, Inc., Burr Ridge, Ill.

Normark, W. R., J. A. Reid, R. W. Sliter, D. Holton, C. E. Gutmacher, M. A. Fisher, and J. R. Childs (1999), Cruise report for O1-99-SC Southern California Earthquake Hazards project, *Open-File Rep. 99–560*, U. S. Geol. Surv., Menlo Park, Calif.

Pares-Sierra, A., and J. O'Brien (1989), The seasonal and interannual variability of the California Currant system: A numerical model, *J. Geophys. Res.*, *94*, 3159–3180.

Peacock, S., C. McCann, J. Sothcott, and T. R. A. Astin (1994), Experimental measurements of seismic attenuation in microfractured sedimentary rock, *Geophysics*, *59*, 1342–1352.

Pike, J. (2000), Data Report: Backscattered electron imagery analysis of early Pliocene laminated Ethmodiscus ooze, Site 1010, *Proc. Ocean Drill. Program Sci. Results*, *167*, 207–212.

Prawirodirdjo, L. M., and Y. Bock (2001), Motions of the California Borderland: Results from the SCIGN array, *Eos Trans. AGU*, *82*(47), Fall Meet. Suppl., Abstract G21A-0952.

Ravelo, A., et al. (1997), Pliocene carbonate accumulation along the California Margin, *Paleoceanography*, *12*(6), 729–741.

Robinson, E. A., T. Durani, and L. Peardon (1986), *Geophysical Signal Processing*, Prentice-Hall, Old Tappan, N. J.

Sams, M. S., J. P. Neep, M. H. Worthington, and M. S. King (1997), Evidence of frequency dependent attenuation in sedimentary rocks, *Geophysics*, *62*, 1–9.

Schon, J. H. (1996), Physical properties of rocks: Fundamentals and principles of petrophysics, in *Handbook of Geophysical Exploration*, Pergamon, New York.

Schopper, J. R. (1982), Porosity and permeability, in *Landolt-Boernstein Numerical Data and Functional Relationships in Science and Technology, Group V: Geophysics and Space Research*, vol. 1, *Physical Properties of Rocks*, pp. 184–303, Springer-Verlag, New York.

Schwalbach, J. R., and D. S. Gorsline (1985), Holocene sediment budgets for the basins of the California continental borderland, *J. Sediment. Petrol.*, *55*, 829–842.

Sheriff, R. E., and L. P. Geldart (1995), *Exploration Seismology*, Cambridge Univ. Press, New York.

Slowey, N., and W. Bryant (1995), Effects of gas and core handling on measurements of compressional wave velocity in Site 893 cores, *Proc. Ocean Drill. Program Sci. Results*, *146*(2), 193–197.

Slowey, N. C., W. R. Bryant, and D. N. Lambert (1996), Comparison of high-resolution seismic profiles and the geoacoustic properties of Eckernförde Bay sediments, *Geo Mar. Lett.*, *16*, 240–248.

Taner, M. T., F. Koehler, and R. E. Sheriff (1979), Complex seismic trace analysis, *Geophysics*, *44*, 1041–1063.

ten Brink, U. S., J. Zhang, T. M. Brocher, D. A. Okaya, K. D. Klitgord, and G. S. Fuis (2000), Geophysical evidence for the evolution of the California Inner Borderland as a metamorphic core complex, *J. Geophys. Res.*, *105*, 5835–5857.

Teng, L. S., and D. S. Gorsline (1991), Stratigraphic framework of the continental borderland basins, southern California, in *The Gulf and Peninsular Province of the California*, edited by P. Dauphin and B. Simoneit, *AAPG Mem.*, *47*, 127–145.

Tuffin, M. D. J., A. I. Best, J. K. Dix, and J. M. Bul (2000) Acoustic characterization of gassy marine sediments, in *Proc. Fifth European Conference on Underwater Acoustics 2000*, pp. 825–830, Eur. Comm., Lyon, France.

Vedder, J. G. (1987), Regional geology and petroleum potential of the southern California borderland, in *Geology and Resource Potential of the Continental Margin of Western North America and Adjacent Ocean Basins-Beaufort Sea to Baja California*, edited by D. W. Scholl, A. Grantz, and J. G. Vedder, *Earth Sci. Ser.*, vol. 6, pp. 403–447, Circum-Pac. Council for Energ. and Mineral Resour., Houston, Tex.

Victor, F. (1997), Outer Borderland province, in *1995 National Assessment of United States Oil and Gas Resources Assessment of the Pacific Outer Continental Shelf Region*, edited by C. Dunkel and K. Piper, *OCS Rep. MMS*, *97–0019*, 151–181.

Ward, S. N., and G. Valensise (1996), Progressive growth of the San Clemente Island, California, by blind thrust faulting: Implications for fault slip partitioning in the California Continental Borderland, *Geophys. J. Int.*, *126*, 712–734.

Widess, M. B. (1973), How thin is a thin bed, *Geophysics*, *38*(6), 1176–1180.

Yilmaz, O. (2001), *Seismic Data Analysis*, *Invest. in Geophys.*, vol. 10, Soc. of Explor. Geophys., Tulsa, Okla.

Zhang, J., U. S. ten Brink, and M. N. Toksoz (1998), Non-linear refraction and reflection travel time tomography: Application to the crustal structure of the California Borderland, *J. Geophys. Res.*, *103*, 29,743–29,757.

A. Janik, Division of Marine Geology and Geophysics, Rosenstiel School of Marine and Atmospheric Science, University of Miami, 4600 Rickenbacker Cswy., Miami, FL 33149, USA. (ajanik@rsmas.miami.edu)

L. M. Liberty and M. W. Lyle, Center for Geophysical Investigation of Shallow Subsurface, Boise State University, Boise, ID 83752, USA. (mlyle@cgiss.boisestate.edu)

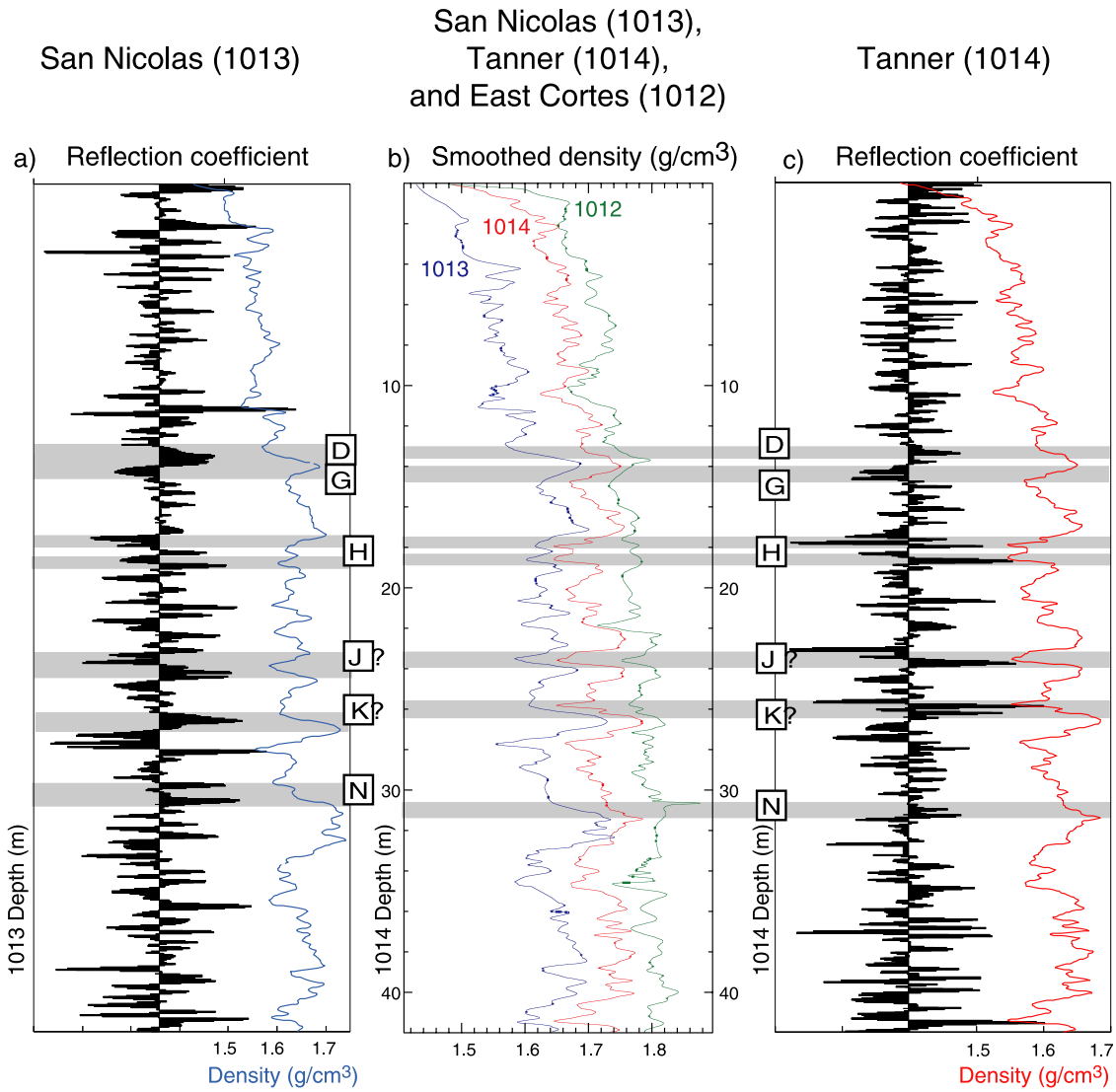

Figure 9. Density and reflection coefficient comparison for the 3 sites. (a) Smoothed density and reflection coefficient profile at Site 1013. Depth scale has been slightly linearly stretched, so 37 mbsf at Site 1013 corresponds to 42 mbsf at Site 1014. (b) Smoothed density profiles at Sites 1013, 1014 (plus 0.1 g/cm^3), and 1012 (plus 0.15 g/cm^3) plotted in an adjusted common depth scale (depth equivalent to Site 1014; depth of Site 1012 adjusted to depth of Site 1014 based on the correlation between stable oxygen isotope data at both sites). Blue, Site 1013; red, Site 1014; and green, Site 1012. (c) Smoothed density and reflection coefficient profile at Site 1014. Gray lines mark the interpreted seismic horizons from 3.5 kHz profiles.

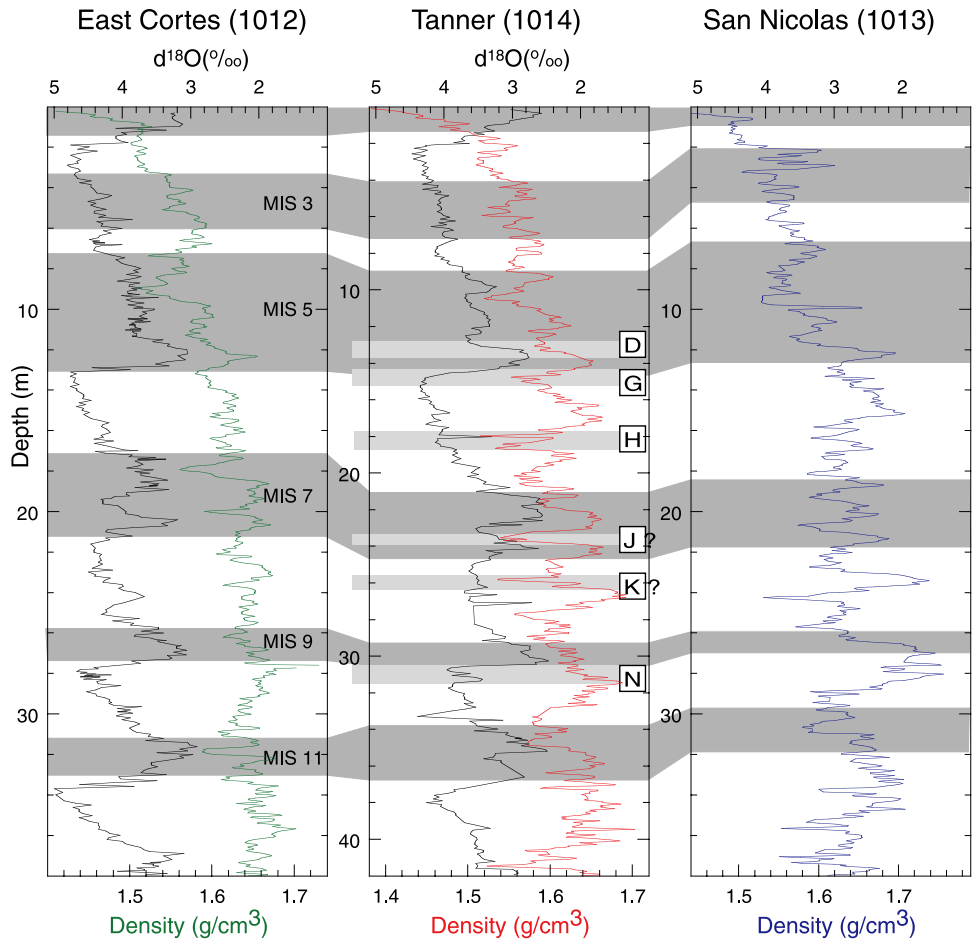

Figure 10. GRAPE density and oxygen isotope data at Sites 1012, 1014, and 1013 [*Hendy and Kennett*, 2000; *Andreasen et al.*, 2000] (A. C. Ravelo, personal communication, 2000). The Marine Isotope Stages (MIS) were marked according to *Imbrie et al.* [1984]. The shaded rectangles show the interpreted position of the reflectors on 3.5 kHz profiles.